Petroleum Science 22 (2025) 2183–2202

Contents lists available at ScienceDirect

Petroleum Science

journal homepage: www.keaipublishing.com/en/journals/petroleum-science

Original Paper

Experimental and modeling investigation of zero net liquid flow in hilly terrain pipeline

Bo Huang [a], Qiang Xu [a, *], Ying-Jie Chang [a], Ye-Qi Cao [a, b], Hai-Yang Yu [a], Yu-Wen Li [a], Lie-Jin Guo [a, **]

[a] State Key Laboratory of Multiphase Flow in Power Engineering, Xi'an Jiaotong University, Xi'an, 710049, Shaanxi, China
[b] College of Petroleum Engineering, Xi'an Shiyou University, 710065, Shaanxi, China

ARTICLE INFO

Article history:
Received 26 August 2024
Received in revised form
28 December 2024
Accepted 21 March 2025
Available online 22 March 2025

Edited by Teng Zhu and Jia-Jia Fei

Keywords:
Hilly terrain pipeline
Zero net liquid flow
Slug flow
Flow pattern transition
Quantitative image processing

ABSTRACT

Hilly terrain pipeline is a common form of pipeline in oil and gas storage and transportation industry. Due to the hilly terrain influence, the liquid at the elbow of the gathering pipeline is easy to flow back and accumulate to form slug flow, so it is necessary to remove the accumulated liquid by gas purging. In this paper, experiment is carried out in hilly terrain pipelines. Three flow patterns of stratified flow, slug flow and stratified entrained flow are observed. The process of gas purging accumulated liquid is divided into four stages, namely liquid accumulation, liquid rising, continuous outflow and tail outflow. At the same time, the flow pattern maps of each stage are drawn. The pressure drop signal is analyzed in time domain and frequency domain, and the contour map of pressure drop distribution is drawn. It is found that the ratio of range to average value can well distinguish the occurrence range of each flow pattern. Based on visualization, the transition process of slug flow to stratified flow and stratified entrained flow is studied, and the transition boundary prediction model is established. An image processing method is proposed to convert the image signal into a similarity curve, and PSD analysis is performed to calculate the slug frequency. The normal distribution is used to fit the slug frequency, and the predicted correlation is in good agreement with the experimental data.

1. Introduction

In the process of oil and gas exploitation and transportation, pipelines are often designed into complex hilly terrain structures due to the influence of terrain changes (Bissor et al., 2020a; Hong et al., 2022; Sunday et al., 2023). Transportation of natural gas through pipelines may be accompanied by liquids such as water, condensate and mono-ethylene glycol (Bissor et al., 2020b). Also, as the temperature and pressure change, the water vapor in natural gas condenses into liquid water (Hong et al., 2020; Fan et al., 2021). They will eventually gather at the elbow of the pipeline, increasing the pressure in the pipeline (He et al., 2018; Bissor et al., 2020b). Once the cross-section is blocked, intermittent flow conditions will occur, such as terrain-induced slugs (Taitel, 1986). In addition, once the slug is formed, it will also aggravate the corrosion of the pipeline and increase the risk of hydrate formation (Deng et al., 2014; Bissor et al., 2020a; Xu et al., 2022). For the UWCAES (underwater compressed gas energy storage systems), once the slug flow occurs, the pressure drop and energy consumption of the system will increase, which will not only affect the gas production efficiency of the pipeline, but also bring security risks (Liang et al., 2023a).

To improve natural gas production, periodic pigging is usually regarded as an efficient accumulated liquid removal method (Minami and Shoham, 1996; Wu et al., 2021). However, when the pipeline diameter is small or the structure is complex, pigging is sometimes difficult to implement (Liu et al., 2021; Zhang et al., 2021). To prevent the pipeline from being damaged, the accumulated liquid at the elbow must be blown out by increasing the gas flow rate (Bissor et al., 2020a). When the gas passes above the accumulated liquid, the gas velocity is not high enough to carry the liquid up. In this case, the liquid only moves upward or downward in the cross section of the pipeline, and does not flow forward. This

* Corresponding author.
** Corresponding author.
E-mail addresses: qiang.xu@mail.xjtu.edu.cn (Q. Xu), lj-guo@mail.xjtu.edu.cn (L.-J. Guo).

https://doi.org/10.1016/j.petsci.2025.03.026

results in a two-phase flow phenomenon in the upward inclined pipe even though the liquid has no initial velocity. Because there is no net liquid flow in the cross-section of the pipe, at this time the flow rate of the inlet and outlet liquid is 0, so this phenomenon is also called zero net liquid flow (Amaravadi et al., 1994).

Compared with the reported literature on gas-liquid two-phase flow, there are few studies on the removal of accumulated liquid with zero net liquid flow. Some researchers have discussed the effect of oil flow on water displacement. Xu et al. (2011) studied the flow of the water carried by oil from a horizontal pipe to an upward-inclined pipe. Researchers (Xu et al., 2012; Mo et al., 2013; Magnini et al., 2018) numerically simulated the phenomenon of oil displacing water. Some researchers have also discharged water by increasing the gas flow rate. Horii et al. (1997) and Shen et al. (2002) studied the phenomenon of accumulated liquid discharged through gas in a U-tube. Gregory et al. (1981) and Amaravadi et al. (1994, 1998) studied the displacement of liquid brought into an upward-inclined pipe by gas. Birvalski et al. (2014) investigated gas carryover of small amounts of water at the bottom in a shallow V-shaped pipe. Yang et al. (2018) simulated the flow process of accumulated liquid in a V-shaped pipe by the action of the gas. Rastogi and Fan (2020) investigated the thickness of the liquid film when the accumulated liquid flows by the action of the gas at different inclination angles and pipe diameters. Liu et al. (2022) studied the gas-carrying capacity in the U-shaped pipe and divided the flow process of the accumulated liquid into four stages. Bissor et al. (2020a) studied the process of completely removing the liquid from the lower section of the pipeline by gas through experiments and simulations, and divided the specific flow stages. Since the zero net liquid flow is still essentially a two-phase flow phenomenon, to judge whether the accumulated liquid has been successfully removed, it is necessary to study the flow stage when the accumulated liquid is discharged from the elbow, and further analyze the relationship between the flow stage and the flow pattern, as well as the change process of the elbow pressure drop.

Slug flow is a common flow pattern in the multiphase flow industry. Researchers have carried out a lot of research on the formation mechanism of slug flow in hilly terrain pipelines, which provides a valuable reference for the problem of zero net liquid flow generated in hilly terrain pipelines. Zheng et al. (1996) found that the liquid slug tended to be stable after entering the upward-inclined pipe, and studied the characteristic parameters such as liquid slug velocity, holdup and film length. Scott and Kouba (1990) established a slug flow model suitable for hilly terrain pipelines, which confirmed that the length of the slug changed greatly when it entered the upward-inclined pipe from the horizontal pipe, but ignored the formation of new slugs at the elbow. Taitel et al. (2016) studied the flow at low superficial gas-liquid velocities in a hilly terrain pipeline. He found a stratified flow in the downward-inclined pipe and a slug flow in the upward-inclined pipe as influenced by the gas. Al Safran et al. (2005) conducted two-phase flow experiments in hilly terrain pipelines with different inclination angles and found two types of slug generation methods, but no process of slug flow generated by convective extrusion was found. Yin et al. (2018, 2020) conducted experiments and numerical simulations on the slug flow in hilly terrain pipelines at low superficial gas-liquid velocities. By comparing with the experimental data, it was found that the slug flow usually occurs at the elbow, and surfactants were used to promote the removal of accumulated liquid loading in hilly terrain pipelines. However, in his research, there is a lack of analysis and calculation of the formation process of slug flow. He et al. (2021) studied the flow transition mechanism of liquid at the elbow of the hilly terrain pipeline. He divided the flow pattern into four types: violent slug flow, bimodal slug flow, oscillating flow and steady flow. Liang et al. (2022, 2023b) studied the formation process and pressure drop of slug flow in the zero net liquid flow. He divided the formation of liquid slug into three types: wave growth, wave aggregation and convective extrusion. By analyzing the thickness of liquid film and the maximum growth factor, a prediction model of critical section speed was established. At the same time, he also established a prediction model for the pressure drop of slug flow applicable to different inclination angles, and the prediction accuracy of the model is ±20%. Zhang et al. (2022) studied the mechanism of liquid slug formation when surfactant was added, and analyzed the influence of inclination angle on slug flow. A method for judging slug generation based on the FFT signal of elbow pressure drop was proposed. However, in order to accurately judge the flow state of the accumulated liquid and ensure the safe operation of the pipeline, it is necessary to study the generation, development and transition process of the slug flow in the zero net liquid flow, establish the corresponding flow pattern transition model, and carry out the prediction of flow characteristics (slug frequency).

When the gas carries accumulated liquid out of hilly terrain pipelines, the instantaneous liquid flow velocity and holdup are unknown. At this time, it is a challenge to model the flow process of transient conditions. Since the liquid flow rate is unknown, the interface of zero net liquid flow will show complex changes, and how to carry out a quantitative study on the flow characteristics of the transient state is also a difficult problem. In this paper, the visualization measurement method is used to study the flow process of accumulated liquid in the hilly terrain pipeline. Firstly, based on the visual image at the elbow, the flow process and flow pattern of the accumulated liquid are divided, and the pressure drop distribution law is given. Secondly, a flow pattern transition model that can predict the occurrence region of slug flow is established. In addition, a quantitative image processing method is proposed, which can deal with the complex transient interface information of zero net liquid flow. Finally, based on the image processing method, the slug frequency of zero net liquid flow is calculated, and the prediction correlation is established.

2. Experimental apparatus and measurement method

2.1. Experimental apparatus

The schematic diagram of the experimental apparatus is shown in Fig. 1. The fluid working media is air and tap water. After being compressed by an air compressor, the gas is measured by a mass flowmeter. The power of the liquid phase is provided by the plunger pump. The liquid and gas phases were measured and entered into a Y-mixer for mixing, then transported to a 46 mm ID experimental section. The experimental pipeline consists of an inlet section, an outlet section and a hilly terrain section. The hilly terrain section adopts the combination of downward-inclined pipe, horizontal pipe and upward-inclined pipe, which is used to simulate the terrain between the mountains. The length of both downward-inclined and upward-inclined pipes is 3.46 m with an inclination angle of 30°, and the horizontal tube is 5.46 m long. The pipeline outlet is connected to the gas-liquid separator. The gas-liquid separator uses the gravity sedimentation method to separate the mixed working fluid. The air is directly discharged into the atmosphere, and the water enters the water tank to achieve recycling. The gas and liquid phase flowmeters are mass flowmeters manufactured by Rheonik of Germany. The gas phase flowmeter is RHM015, the measurement range is 0–20.0 kg/min, and the measurement accuracy is ±0.50%. The liquid phase flowmeter is RHM15, the measurement range is 0–150 kg/min, and the measurement accuracy is ±0.15%. There is a water injection port at the

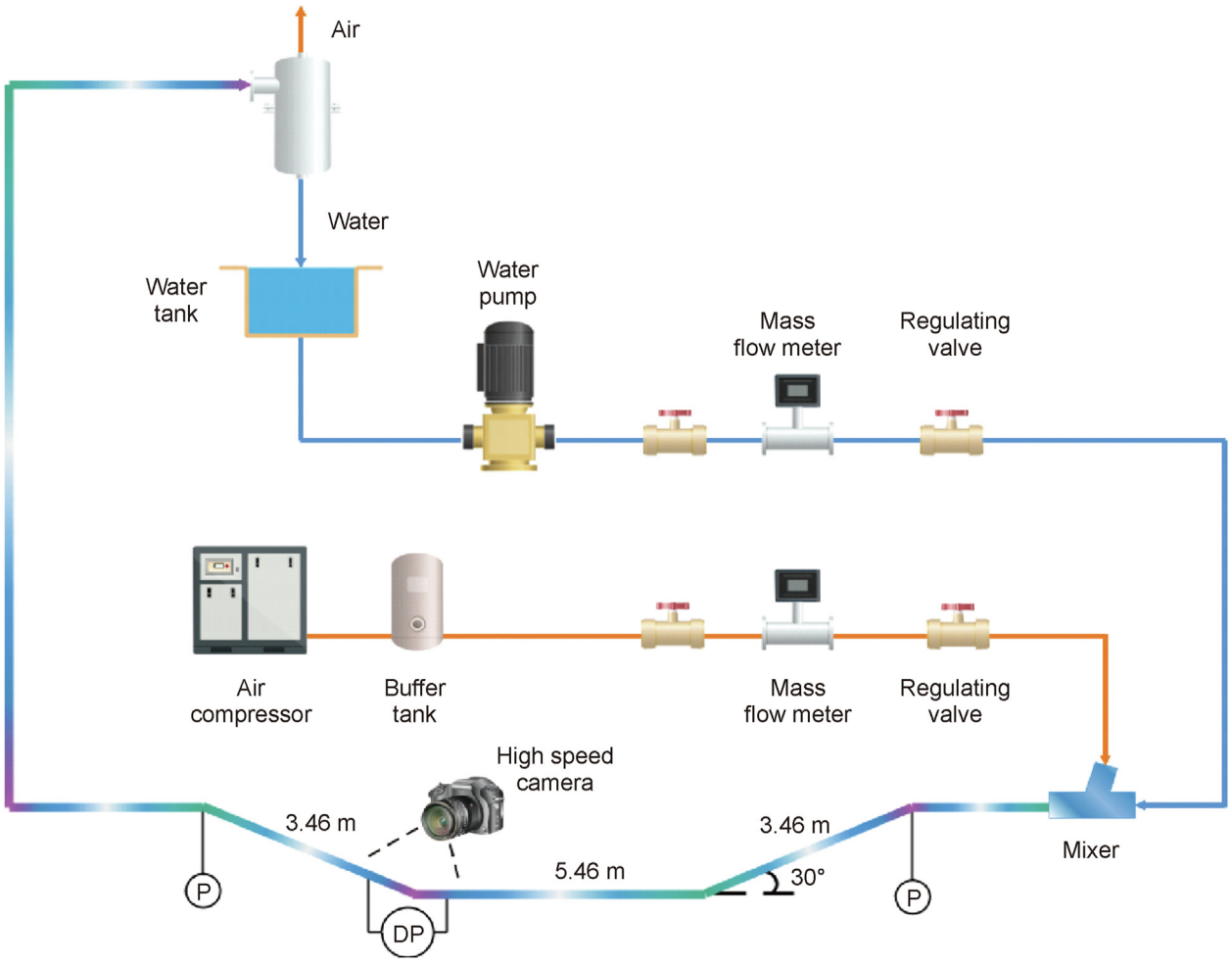

Fig. 1. The schematic diagram of the experimental apparatus.

top of the horizontal pipe in the hilly terrain section. A certain volume of water was injected into the pipe to simulate the accumulated liquid flow in the horizontal section of the hilly terrain pipeline. The volume of the horizontal pipe in the hilly terrain section is V, and the volume of water added is V_L, then the initial liquid holdup is $H_L = V_L/V$. The range of superficial gas velocity V_{SG} is 1.0–22.0 m/s, and the range of initial liquid holdup H_L is 0.15–0.8. The experiment in this paper covers the amount of accumulated liquid in different conditions of low, medium and high.

Two pressure sensors are installed at the entrance of the downward-inclined pipe and the exit of the upward-inclined pipe respectively to measure the pressure here. A pressure difference sensor is installed at the elbow connection between the horizontal pipe and the upward-inclined pipe to measure the pressure drop here. The pressure measurement uses the YOKOGAWAEJA530E pressure sensor produced by the Japanese Yokogawa company. The range is 0–100 kPa, and the measurement accuracy is ±0.075%. The pressure difference measurement uses the ROSEMOUNT3051SD pressure difference sensor produced by the American ROSEMOUNT company. The range is 0–6 kPa, and the measurement accuracy is ±0.075%. A high-speed camera is placed at the elbow to capture the flow process in the visualization window. The high-speed camera is a FASTCAM Mini with a resolution of 2048 × 2048 pixels and a frame rate of 250 fps. The lens used is Nikon f/1.8 D, and the shutter speed is 1/6000 s. Before the experiment, pure water is added to the visualization window to reduce the scattering of light on the pipe wall.

2.2. Measurement method

2.2.1. Cosine similarity processing method based on gray histogram

If a method can be invented, the image signal can be transformed into a certain eigenvalue, and there is a unique mapping relationship between each image and the eigenvalue. In this way, the image signal with a large amount of data can be transformed into a time series curve with oscillation similar to the differential pressure signal, and it will be possible to process the image data quickly and accurately. In this paper, a cosine similarity processing method based on gray histogram is developed, which can fully realize the above functions. Based on this method, a series of input visual images can be transformed into periodic similarity curves after processing.

(1) The flow visual images for a given superficial gas-liquid velocity are entered into the MATLAB program and each image is read and stored, and the initial image is shown in Fig. 2(a).
(2) Set the cropping matrix to crop the initial image. After cropping, the parts unrelated to the flow have been completely removed, as shown in Fig. 2(b).
(3) A grayscale histogram is generated for the cropped image, as shown in Fig. 2(c).

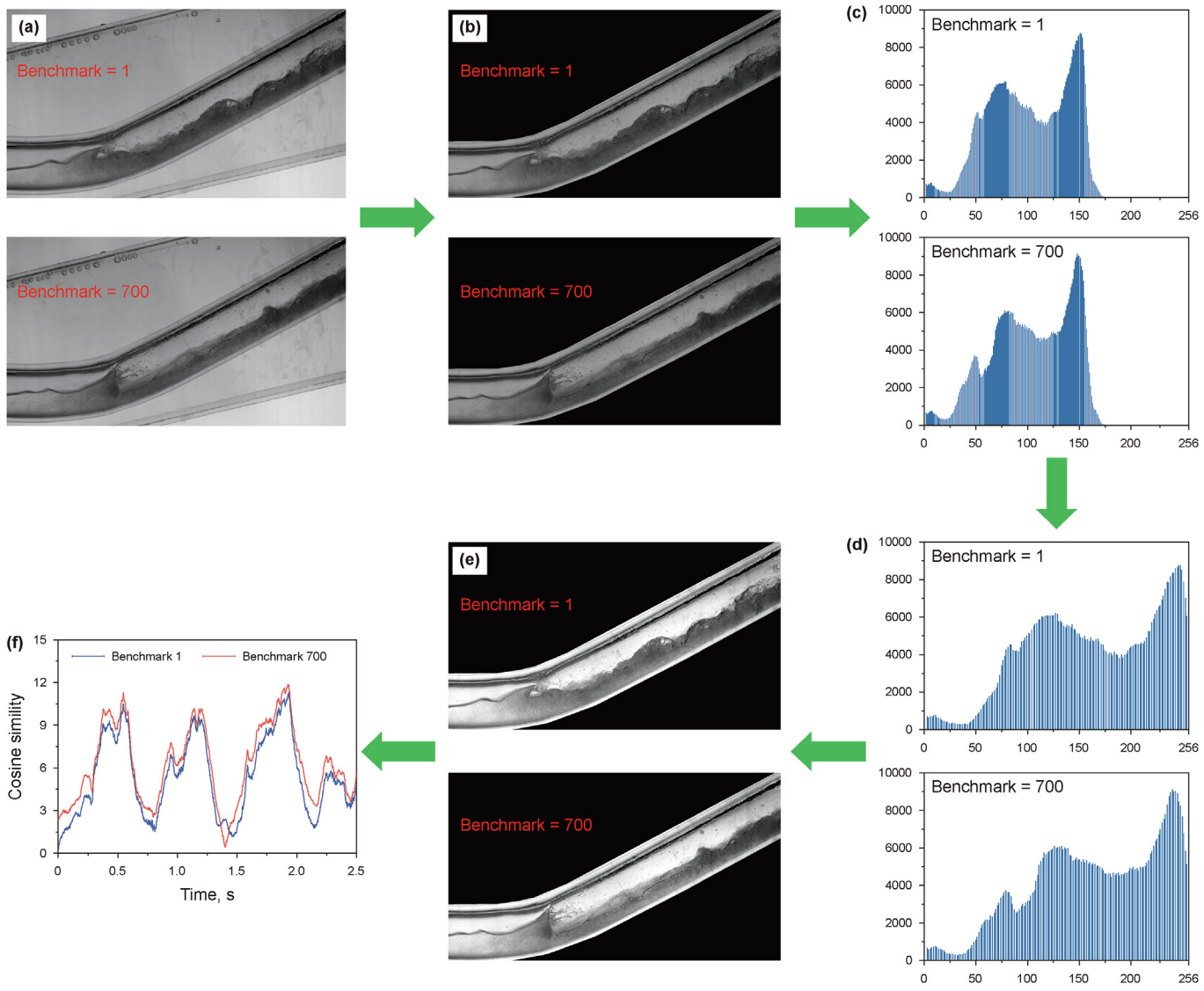

Fig. 2. Image similarity process for grayscale histograms (H_L = 0.15, V_{SG} = 5.0 m/s). (**a**) Initial images; (**b**) Image cropping; (**c**) Generate a grayscale histogram; (**d**) Grayscale histogram region expansion; (**e**) Images after stretching; (**f**) Similarity curve.

(4) Gray scale transformation is performed and the histogram is equalized. It can be seen from Fig. 2(d) that the histogram is extended on the entire gray level (256 levels) compared to Fig. 2(c).
(5) Each histogram is divided into 64 regions, and each region is divided into 4 consecutive gray levels. By summing the gray values of each region, the obtained data is generated into an n-dimensional vector.
(6) According to the steps [1, 2, 3, 4, 5], all the input images are converted into vectors M_i (i = 1, 2, 3 … …). One of the visual images is taken as the benchmark M_0. To facilitate the calculation, the first photo is selected as the benchmark at each superficial gas-liquid velocity. The cosine similarity between the vector M_i and the benchmark M_0 is calculated one by one, and the similarity curve shown in Fig. 2(f) is obtained.

It can be seen from Fig. 2(f) that when the 1st and 700th images are used as the benchmarks, the shapes of the similarity curves are close. To quantitatively describe the differences in the time domain of similarity signals with different benchmarks, the change process of time domain eigenvalues with benchmarks is drawn, as shown in Fig. 3. It can be found that the time domain eigenvalues (mean, maximum and extremum difference) show random variations with benchmarks, and the time domain eigenvalues of different benchmarks are not the same.

2.2.2. Probability density function (PDF) and power spectrum density (PSD)

The probability density function (PDF) is often used to distinguish different two-phase flow patterns (Kaji et al., 2009; Abdulkadir et al., 2014). The relative probability density distribution of a set of discrete data is:

$$\mathrm{PDF}(x_1 < X < x_2) = \int_{x_1}^{x_2} p(x)\mathrm{d}x \tag{1}$$

where x_1 and x_2 are the lower and upper limits of the statistical intervals, respectively. The number of statistical intervals in this paper is calculated as follows:

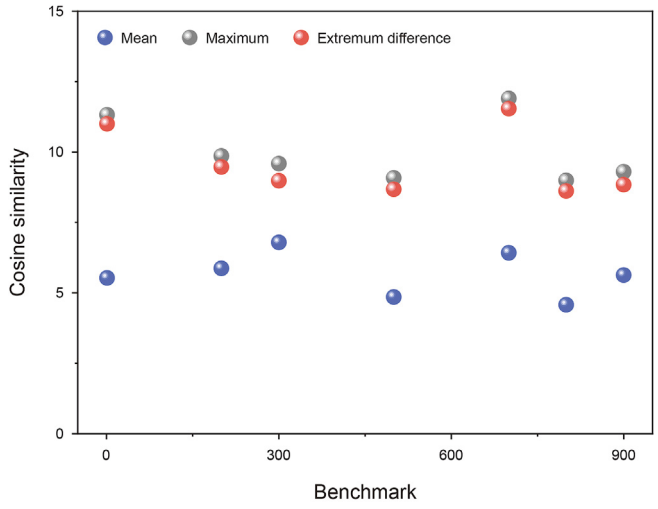

Fig. 3. Variation of time domain eigenvalues with benchmarks. (H_L = 0.15, V_{SG} = 5.0 m/s).

$$N = 1.87(n-1)^{0.4} \tag{2}$$

where n is the total number of data points and N is the number of statistical intervals. The size of the statistical interval is:

$$x_2 - x_1 = (p_{max} - p_{min}) / N \tag{3}$$

Power spectrum density (PSD) is a probabilistic statistical method. It represents the distribution characteristics of signal power with frequency, and is an indicator of the mean square value of random variables. The power spectrum density estimation can be obtained by the Fourier transform of random signal sequence. The calculation equation is as follows:

$$S_x(\omega) = \frac{1}{N}\left|X\left(e^{j\omega}\right)\right|^2 \tag{4}$$

where $X(e^{j\omega})$ is the discrete Fourier transform of the signal, which is calculated as follows:

$$X\left(e^{j\omega}\right) = \sum_{n=0}^{N-1} x(n)e^{-j\omega n} \tag{5}$$

The slug frequency f_s is the number of times a liquid slug passes through a fixed position in the pipe over a while and can be expressed as:

$$f_s = \frac{N}{\Delta t} \tag{6}$$

where N is the number of liquid slugs passed and Δt is the time interval between the first and the last liquid slugs passing through the fixed position.

It has been pointed out in the published literature that the slug frequency can be obtained by the PSD analysis method for intermittent flow with periodic time series signals (Arabi et al., 2020; Yu et al., 2023). Fig. 4 shows the PSD analysis results of similarity signals at different superficial gas velocities when H_L = 0.15. The value of cosine similarity can quantify the degree of change in the phase interface. It can be seen that when the superficial liquid velocity is 1.0 m/s, the accumulated liquid at the elbow is in a static state, the PSD value is less than 0.01, and the signal is stable, indicating that the energy is extremely low at this time, and the gas-liquid interface almost does not fluctuate. When the superficial liquid velocity is 5.0 m/s, the similarity signal has obvious periodic changes, the maximum value is 10, and the interface changes very violently. The PSD signal shows a single-peak distribution with a unique dominant frequency, which is the slug frequency.

To quantitatively describe the differences in the frequency domain of the similarity signals of different benchmarks, the change process of frequency domain eigenvalues with benchmarks is drawn as shown in Fig. 5. Combined with Figs. 3 and 5 and Table 1, it can be seen that although the mean value, maximum value and extremum difference change randomly with benchmarks in the time domain, the mean value is similar in the frequency domain, and even the dominant frequency is constant. Therefore, the first image of each superficial gas-liquid velocity condition can be used as a benchmark when analyzing the dominant frequency of the slug flow using the image similarity method. This enables a lot of time savings and makes it possible to process a large number of image data quickly.

2.3. Uncertainty analysis

2.3.1. Error analysis caused by visualization window

In this paper, visualization analysis is used in experimental measurements. The difference of refractive index in different media leads to the deflection of parallel light, which is the main source of error in visualization analysis.

Fig. 6 shows the process of error caused by the propagation of parallel light in a circular pipe. The refractive index of light in PMMA is 1.49, the refractive index of water is 1.33, and the refractive index of air is 1.00. After entering the visualization window, the parallel light first passes through the outer wall of the pipe, and then passes through the inner wall of the pipe. In Fig. 6, L represents the position of the incident parallel light relative to the center of the pipe. The incident angle of the outer wall of the pipe is α_1, the refractive angle is α_2, the incident angle of the inner wall of the pipe is β_1, and the refractive angle is β_2. θ is the angle between the deflected light passing through the 5 mm wall thickness and the center of the pipe, and S is the position of the deflected light relative to the center of the pipe. The specific calculation process is as follows. Taking the example of filled water, when parallel light shines on the outer wall of the pipe, the law of refraction is satisfied, so there is:

$$1.33\ \sin\alpha_1 = 1.49\ \sin\alpha_2 \tag{7}$$

The refraction angle α_2 of the outer wall of the pipe and the incident angle β_1 of the inner wall of the pipe satisfy:

$$\alpha_2 = \beta_1 - \theta \tag{8}$$

As the light passes through the inner wall of the pipe, the relationship is satisfied:

$$1.49\ \sin\beta_1 = 1.33\ \sin\beta_2 \tag{9}$$

From the trigonometric function relationship, it can be obtained:

$$\sin\alpha_1 = \frac{L}{R_{out}} \tag{10}$$

$$S = R_{in}\ \sin(\alpha_1 + \theta) + R_{in}\cos(\alpha_1 + \theta)\tan(\beta_2 - \alpha_1 - \theta) \tag{11}$$

Substituting Eqs. (11)–(14) into Eq. (15) solves for S. The equation of the relative error is:

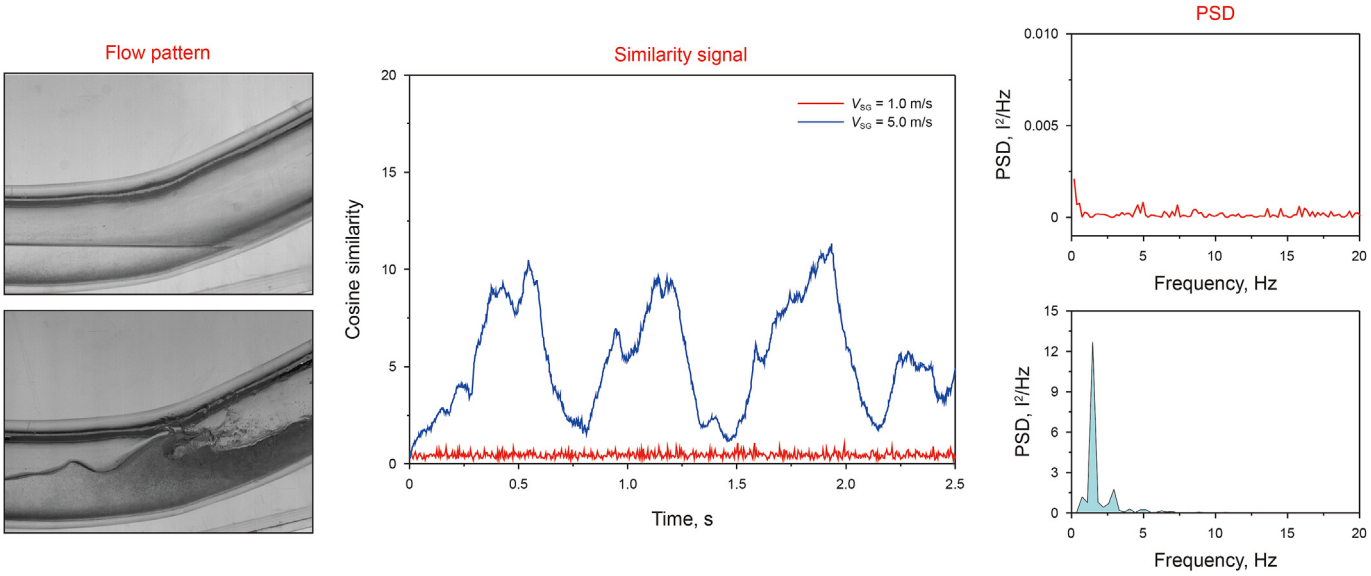

Fig. 4. PSD analysis results of similarity signals at different superficial gas velocities. (H_L = 0.15).

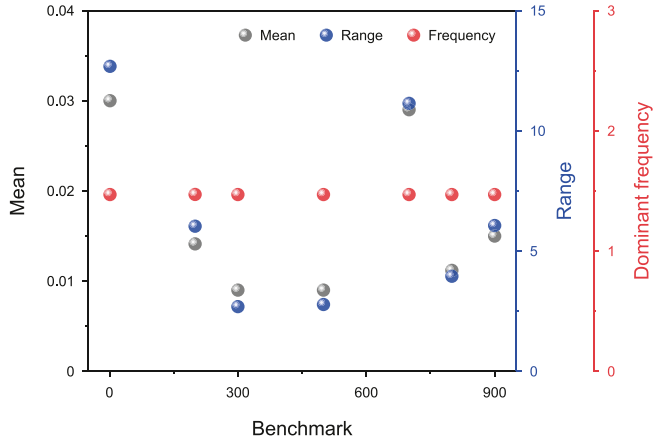

Fig. 5. Variation of frequency domain eigenvalues with benchmarks. (H_L = 0.15, V_{SG} = 5.0 m/s).

$$Error = \frac{L-S}{L} \times 100\% \tag{12}$$

Fig. 6(b) and (c) are the calculation results of the relative error for L = 14 mm and $\alpha_1 = 30°$ when the visualization window is not filled with water and filled with water, respectively. The relative error is 24.21% when not filled with water, and the relative error is 0.02% when filled with water.

Fig. 7 further compares the relative errors in the range of 0–1.0 R when filled with water and unfilled with water. It is found that for parallel light incident at any position, the relative error of water-filled is much smaller than that of water-unfilled. Therefore, filling the visualization window with water before the experiment can effectively reduce the measurement error, and the mean of the error is 1.11%.

2.3.2. Uncertainty of measurement data

It is necessary to analyze the uncertainty of the measurement data in the experiment. Moffat (1988) gave the calculation method of uncertainty of measurement data. The uncertainty of direct measurement data is:

$$x_t = x \pm \delta x \tag{13}$$

where x_t is the true value, x is the experimental value, and δx is the maximum absolute error. There is a functional relationship between indirect measurement data and direct measurement data as follows:

$$y = f(x_1, x_2, \ldots\ldots, x_i) \tag{14}$$

where y is the indirect measurement data and x_i is the direct measurement data, i = 1, 2, …, n. The maximum absolute error of indirect measurement data is:

Table 1
Comparison of time-domain and frequency-domain eigenvalues at different benchmarks.

Benchmark	Time domain eigenvalues			Frequency domain eigenvalues			
	Mean	Max	Range	Mean	Max	Range	Dominant frequency
1	5.53	11.32	11.00	0.03	12.68	12.68	1.47
200	5.87	9.86	9.47	0.01	6.03	6.03	1.47
300	6.79	9.59	8.98	0.01	2.69	2.69	1.47
500	4.85	9.08	8.68	0.01	2.78	2.78	1.47
700	6.42	11.90	11.54	0.03	11.14	11.14	1.47
800	4.58	8.99	8.62	0.01	3.95	3.95	1.47
900	5.63	9.30	8.84	0.02	6.06	6.06	1.47

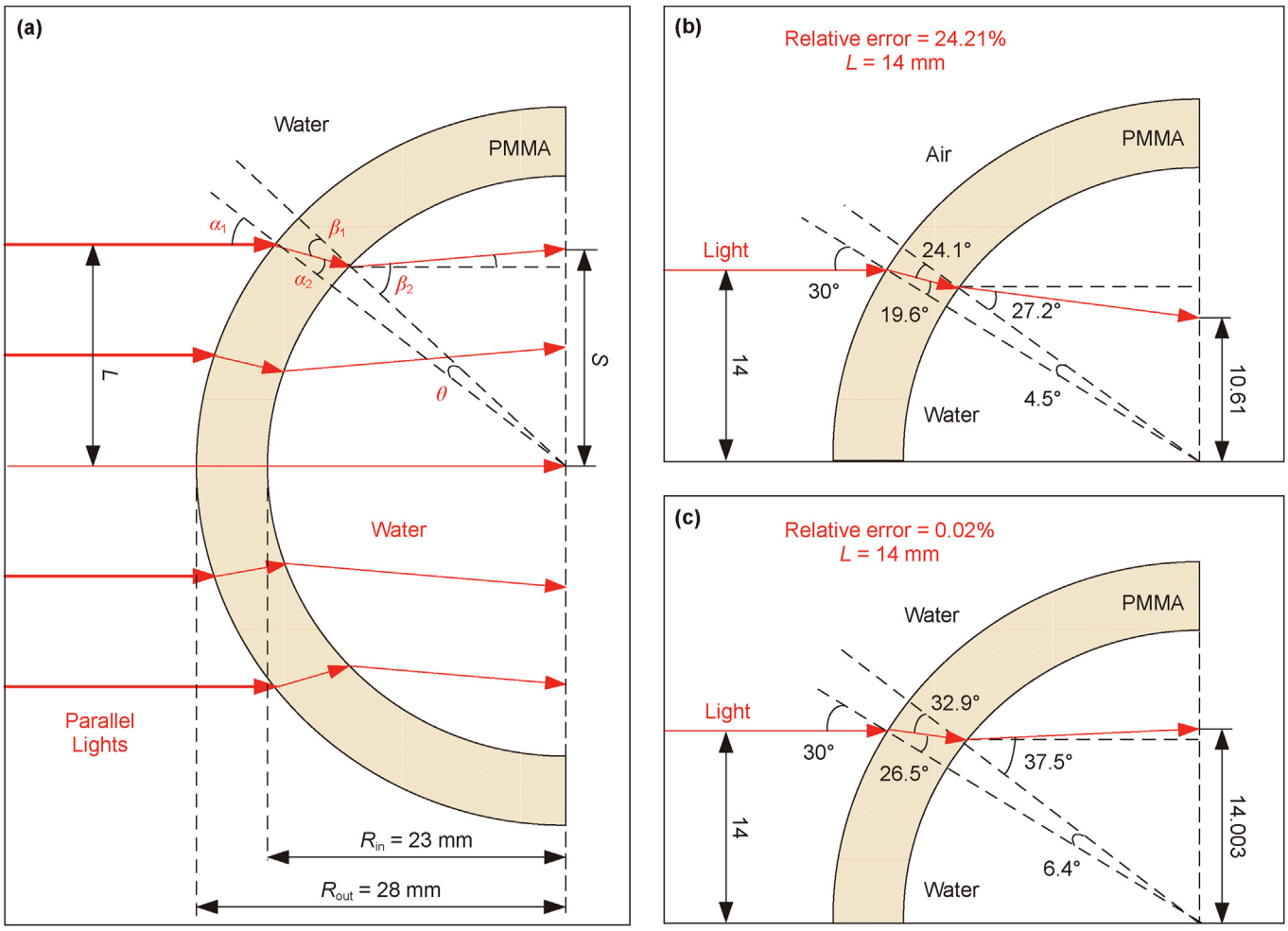

Fig. 6. Uncertainty analysis in visualization analysis (green rectangle represents visualization window). (**a**) The uncertainty calculation process of the visualization window; (**b**) The visualization window is not filled with water; (**c**) The visualization window is filled with water.

$$\delta y = \sum_{i=1}^{n} \left| \frac{\partial f}{\partial x_i} \delta x_i \right| \tag{15}$$

The relative uncertainty is:

$$u = \frac{\delta y}{\bar{y}} \tag{16}$$

where δy is the absolute error of the indirect measurement data, and δx_i is the absolute error of the direct measurement data, $\bar{y}$ is the mean of the measurement results, and u is the relative uncertainty. The measurement data in this paper, such as the gas phase volume flow rate, pressure and pressure drop, are measured with an accuracy determined by the sensor. Measurement of the slug frequency is derived from the visualization, and the error analysis of the visualization is given in Section 2.3.2. The calculation process and results of the above data uncertainty are shown in Table 2.

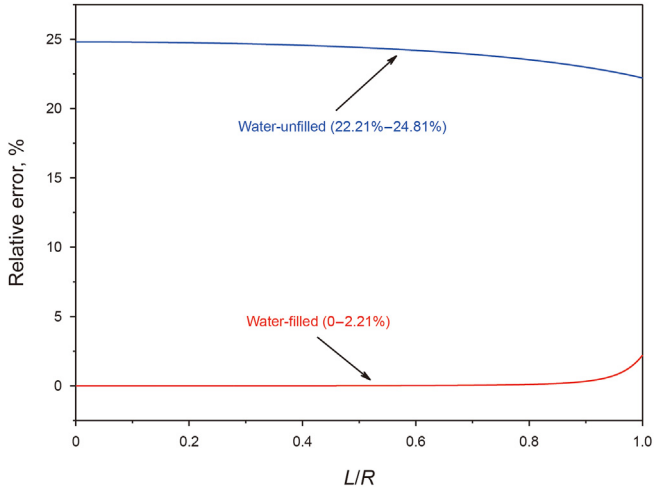

Fig. 7. Comparative analysis of relative errors in the visualization window between filled with water and unfilled with water.

3. Results and discussion

3.1. Flow stages and flow patterns of fluid accumulation

Bissor et al. (2020a) pointed out that the process of accumulated liquid from static to complete discharge in zero net liquid flow is divided into four stages: (1) The transition from smooth stratified flow to wavy stratified flow in a horizontal pipe. (2) The horizontal pipe partially dried up, and the accumulated liquid gradually

Table 2
Uncertainty analysis of measurement data.

Measurement data	Range	Calculation equation of uncertainty	Relative uncertainty, %
Superficial gas velocity	0–20 kg/min	$u(V_{SG}) = \frac{\delta(V_{SG})}{\overline{V_{SG}}}$	6.7
Pressure	0–100 kPa	$u(P) = \frac{\delta(P)}{\overline{P}}$	1.4
Pressure drop	0–6 kPa	$u(\Delta P) = \frac{\delta(\Delta P)}{\overline{\Delta P}}$	0.2
Slug frequency	0–5 Hz	$u(f_s) = \frac{\delta(f_s)}{\overline{f_s}}$	3.7

moved to the elbow and penetrated into the upward-inclined pipe. (3) The horizontal pipe completely dried up. (4) The accumulated liquid in the hilly terrain section is completely removed. The flow process of liquid accumulation in the hilly terrain pipeline is related to the phenomenon of multiphase flow, which is essentially presented by the flow pattern. Therefore, in this paper, the flow pattern was studied while the flow stage was divided.

The accumulated liquid must pass through the elbow when it flows from the horizontal pipe to the upward-inclined pipe. Therefore, in this paper, the flow process of fluid accumulation in the hilly terrain pipeline is divided into four stages based on the visual images and pressure drop signals at the elbows: (1) liquid accumulation; (2) liquid rising; (3) continuous outflow; (4) tail outflow.

Liquid accumulation: The schematic diagram of this stage is shown in Fig. 8(a). When the superficial gas velocity is low, the friction between gas and liquid is not enough to make the accumulated liquid flow. The gas-liquid interface at the elbow is stable, and the liquid film height increases slowly with the action of the gas. If the superficial gas velocity is slightly increased at this time, the gas-liquid interface will start to wave because the liquid cannot enter the upward-inclined pipe. In this stage, the flow pattern of the elbow is smooth stratified flow and wavy stratified flow. From the pressure drop signal, it can be seen that the elbow is stratified flow at this time, and the mean and extremum difference of pressure drop are very small.

Liquid rising: The schematic diagram of this stage is shown in Fig. 8(b). The superficial gas velocity at this stage is greater than that at the liquid accumulation stage. The accumulated liquid will move to the upward-inclined pipe with the action of gas and begin to rise. However, due to the lack of kinetic energy, it will begin to backflow when it rises to a certain height. After the backflow collides with the incoming flow, the originally flat interface will generate an interface wave, and the liquid will enter the upward-inclined pipe again, which is repeated.

Continuous outflow: The schematic diagram of this stage is shown in Fig. 8(c). The superficial gas velocity at this stage is greater than that at the liquid rising stage. The liquid film is carried out of the upward-inclined pipe with the action of gas without backflow, and the liquid flows out continuously at this time. The liquid is sheared into small droplets and dispersed in the gas core with the action of gas. The droplets further impact the top of the pipe and deposit, forming an annular liquid film on the pipe wall. In this stage, the flow pattern of the elbow is slug flow. Due to the existence of an annular liquid film, it also has the characteristics of annular flow. Compared with the liquid rising stage, the fluctuation of the pressure drops signal decreases, the mean value increases, and the extremum difference decreases.

Tail outflow: The schematic diagram of this stage is shown in Fig. 8(d). The whole accumulated liquid can be regarded as a huge liquid film. At this stage, the tail of the liquid film begins to move, and finally completely moves out of the upward-inclined pipe. The liquid holdup at this stage is very low, and a stable annular liquid film cannot be formed. At this time, the liquid moves against the wall of the lower pipe, and the tail liquid film has to overcome the huge liquid wall friction and gravity during the rising process. Compared with the continuous outflow stage, the pressure drop signal is very stable, with little change in the mean value but a decrease in the extremum difference.

To understand the complete flow process of the accumulated liquid, the flow pattern maps of the horizontal pipe, the upward-inclined pipe and the elbow are drawn as shown in Fig. 9. There are three types of flow patterns in this paper: stratified flow (SF), slug flow (SG) and stratified entrained flow (SEF). The stratified flow includes two sub-flow patterns: smooth stratified flow (SS) and stratified wavy flow (SW), and the slug flow includes two sub-flow patterns: slug flow (SG) and pseudo-slug flow (PSG). It should be noticed that unlike stratified flow, stratified entrained flow contains entrained droplets in the gas phase. The concentration of entrained droplets decreases from bottom to top (Lei, 2015). Due to the low liquid holdup, the entrained droplets cannot form a circumferential liquid film. Two concepts are defined before introducing the flow pattern map: no-flow zone and co-flowing zone. The no-flow zone means that the effusion has dried up and no liquid exists. The co-flow zone means that the accumulated liquid is not dried up, and the flow range of the liquid covers the horizontal pipe, the upward-inclined pipe and the elbow.

It can be seen from Fig. 9(a) that only smooth stratified flow and wavy stratified flow occur in the horizontal pipe. When the superficial gas velocity is in the range of the co-flow zone, the smooth stratified flow transitions to wavy stratified flow. Increasing the superficial gas velocity in the horizontal pipe, the liquid accumulation stage changes to the liquid rising stage, and they take the co-flow zone as the dividing line. It is worth noting that the wavy stratified flow in the co-flow zone of the horizontal pipe is caused by the backflow of the upward-inclined pipe, so an interface wave of reverse transmission will be generated. The wavy stratified flow in the co-flow zone flows upstream, which is represented by SW(−) because it is reverse. The wavy stratified flow in the no-flow zone flows downstream, represented by SW(+).

It can be seen from Fig. 9(b) that only slug flow and stratified entrained flow occur in the upward-inclined pipe. Different from the horizontal pipe, the flow in the upward-inclined pipe starts from the co-flow zone, that is, the initial stage is the liquid rising. When the superficial gas velocity is greater than the range of the co-flow zone, the flow changes from the liquid rising stage to the continuous outflow stage. Continue to increase the superficial gas velocity, the upward-inclined pipe flow pattern transitions from slug flow to stratified entrainment flow, and the continuous outflow stage changes to the tail outflow stage.

There is no flow zone in both horizontal and upward-inclined pipes, so their flow pattern maps are incomplete. However, the

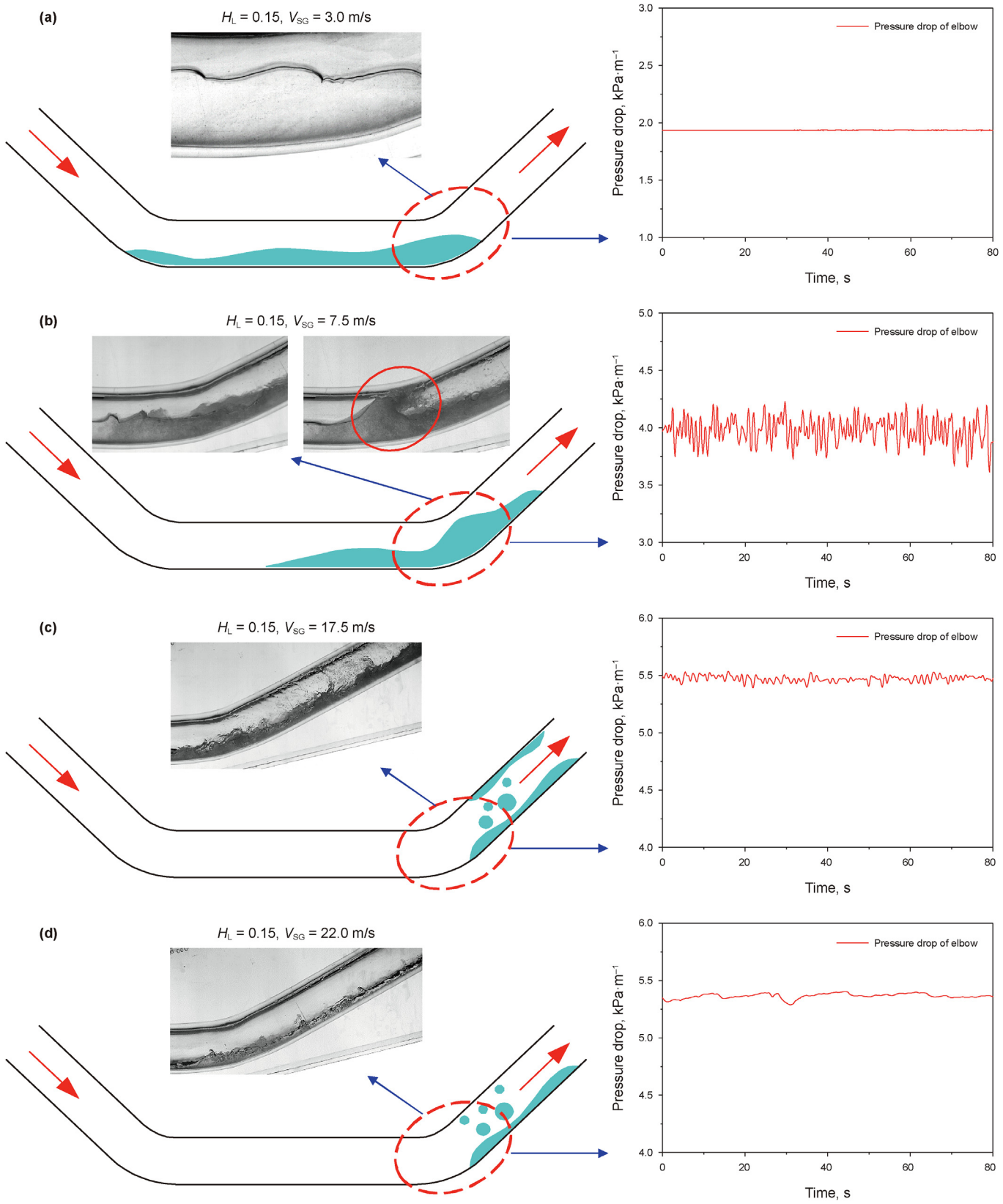

Fig. 8. Flow stages of accumulated liquid at the elbow. (**a**) Liquid accumulation; (**b**) Liquid rising; (**c**) Continuous outflow; (**d**) Tail outflow.

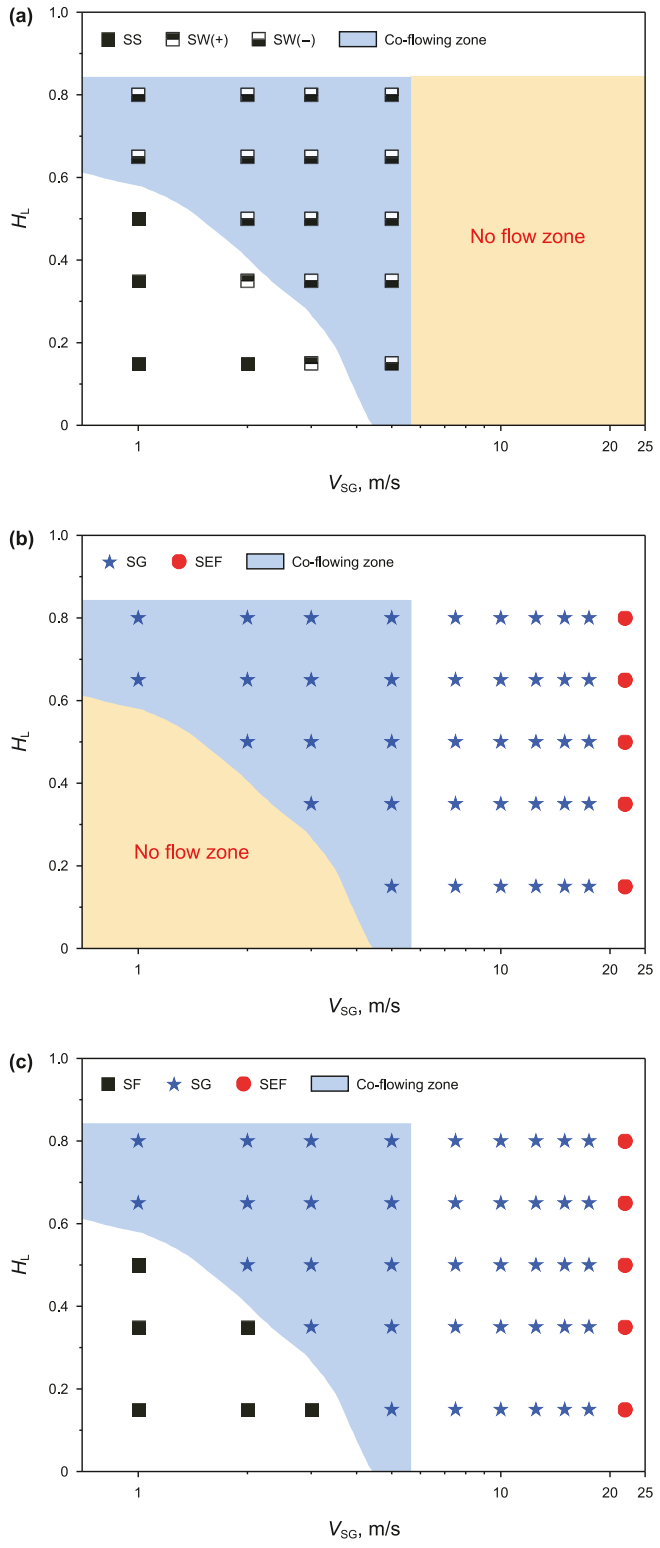

Fig. 9. Flow pattern in the process of accumulated liquid. (**a**) Horizontal pipe; (**b**) Upward-inclined pipe; (**c**) Elbow.

flow pattern map at the elbow is complete, as shown in Fig. 9(c). There are three flow patterns at the elbow: stratified flow (SF), slug flow (SG) and stratified entrained flow (SEF). Starting from the superficial gas velocity of 1 m/s, when the superficial gas velocity is increased to the range of the co-flow zone, the liquid accumulation

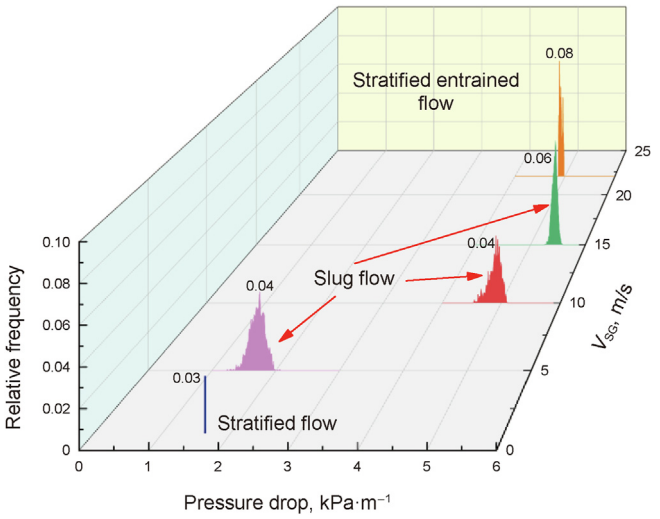

Fig. 10. Variation of elbow pressure drop PDF with superficial gas velocity ($H_L = 0.15$).

stage becomes the liquid rising stage. When the superficial gas velocity is greater than the range of the co-flow region, the liquid rising stage becomes the continuous outflow stage. Continue to increase the superficial gas velocity, the flow pattern transitions to stratified entrained flow, and the continuous outflow stage becomes the tail outflow stage. By analyzing the flow pattern map of the elbow, the flow stages and flow patterns of accumulated liquid are related. In this way, the occurrence regions of different flow patterns are visually displayed, which provides an important reference value for the later study of the flow pattern transition mechanism.

3.2. Pressure drop characteristics of elbow

The PDF distribution of the pressure drop signal can be used as an important basis for distinguishing different flow patterns (Yu et al., 2023). To further understand the flow characteristics at the elbow, the pressure drop signal of the elbow was studied in this paper. The variation of the PDF distribution of the pressure drop signal with the superficial gas velocity is shown in Fig. 10. It can be seen that when $V_{SG} = 1$ m/s, the flow pattern at the elbow is stratified flow, and its PDF presents a single-peak columnar structure. When the superficial gas velocity is 5, 10 and 15 m/s, the flow pattern is slug flow, and the PDF is normal distribution. When the flow pattern is slug flow, increasing the superficial gas velocity, the PDF distribution area gradually changes to a higher-pressure range. When the superficial liquid velocity increases to 22 m/s, the flow pattern transitions to stratified entrained flow, and the PDF is a pinprick. Compared with slug flow, the distribution area of PDF moves to the left (pressure drop decreases). The fluctuation range of pressure drop satisfies slug flow > stratified entrained flow > stratified flow, which also shows that slug flow is the most unstable flow pattern.

The time series of the pressure difference signal is transformed into the frequency domain, which can analyze the freqency domain characteristics and extract the relevant characteristic parameters (Nnabuife et al., 2021a, 2021b). In this paper, the PSD of pressure drop signals at different superficial gas velocities is analyzed, as shown in Fig. 11. It can be seen that the fluctuation of the stratified flow interface is small, and the frequency domain spectrum signal obtained by Fourier transform is very stable and basically remains unchanged. At any superficial gas velocity, the frequency domain signal of slug flow is always distributed in the frequency domain of

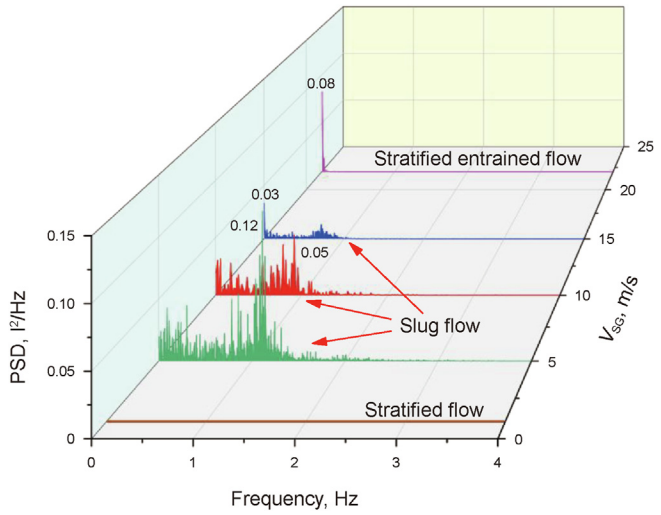

Fig. 11. Variation of elbow pressure drops PSD with superficial gas velocity ($H_L = 0.15$).

0–4 Hz. When the superficial gas velocity increases, the signal intensity of the slug flow increases first and then decreases. When the superficial liquid velocity $V_{SG} = 5.0$ m/s, the signal intensity reaches the maximum. The dominant frequency corresponding to the maximum signal intensity also increases first and then decreases, and the dominant frequency reaches the maximum when $V_{SG} = 5.0$ m/s. When the flow pattern transitions to stratified entrained flow, the slug disappears, and its frequency domain signal distribution range is between 0 and 0.5 Hz, indicating that the fluctuation degree becomes smaller, but the energy density increases and becomes more concentrated.

From the above analysis, it can be found that the flow pattern is affected by the superficial gas velocity, and different flow patterns have different pressure drop fluctuation characteristics. To investigate the effect of initial liquid holdup and superficial gas velocity on pressure drop, the contour map of pressure drop distribution is drawn as shown in Fig. 12. Fig. 12(a) shows a contour map of the mean of the pressure drop at the elbow, where the mean of the pressure drop can indicate the difficulty of the accumulated liquid leaving the elbow. It can be seen that the mean of pressure drop increases with the superficial gas velocity increases. However, when the initial water holdup increases, the mean of pressure drop does not change significantly. As the initial liquid holdup increases, the area where the mean of pressure drop exceeds 4.40 kPa (the red area in Fig. 12(a)) continues to decrease. This indicates that the higher the initial water holdup, the easier the accumulated liquid enters the liquid rising stage from the liquid accumulation stage and flows out of the upward-inclined pipe in the form of slug flow.

The pressure drop signals of different flow patterns are different. This is not only reflected in the mean of pressure drop, but also in the fluctuation range of pressure drop. Therefore, to accurately represent the range of each flow pattern on the contour map, the mean and fluctuation ranges need to be considered. Here is a dimensionless number-the inhomogeneity value of pressure drop (Xu et al., 2020, 2021), which is defined as:

$$Ra = \frac{\Delta P_{\text{Range}}}{\Delta P_{\text{m}}} = \frac{\Delta P_{\text{max-min}}}{\Delta P_{\text{m}}} \tag{17}$$

where ΔP_{Range} denotes the extremum difference, $\Delta P_{\text{Range}} = \Delta P_{\text{max}}$ (maximum) $- \Delta P_{\text{min}}$ (minimum), as shown in Fig. 12(b). It can be seen from the contour map of the pressure drop inhomogeneity that the blue region on the lower left and right is the region with the smallest inhomogeneity value. The lower left corner of Fig. 12(b) is the stratified flow region, and its inhomogeneity value is less than 0.12. The right side of Fig. 12(b) is a stratified entrained flow region with an inhomogeneity value of less than 0.07. The remaining region is the range where slug flow occurs, with inhomogeneity values ranging from 0.12 to 0.54. The largest value of inhomogeneity occurs in the co-flow zone (red part in Fig. 12(b)). Since the liquid slug generated at the elbow transmits pressure fluctuations both to the horizontal pipe and upward-inclined pipe, the co-flow zone has the largest value of inhomogeneity.

3.3. Flow pattern transition

The analysis in Section 3.1 shows that the flow stage of the accumulated liquid is closely related to the flow pattern. The flow pattern in the liquid accumulation stage is stratified flow and in the tail outflow stage is stratified entrained flow. The slug flow is an unstable flow state, which will cause periodic outflow of accumulated liquid in the pipe. The slug flow of zero net liquid flow is essentially topographically induced (Zhang et al., 2022). In this paper, there are two kinds of slug flow found in the experiment,

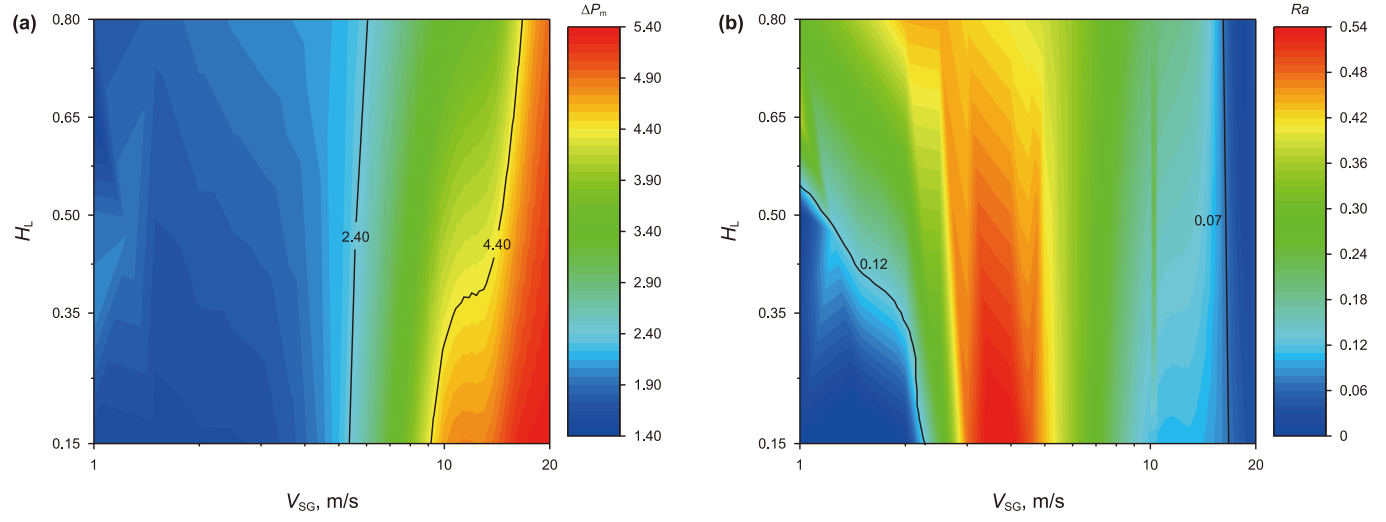

Fig. 12. Contour map of pressure drop at elbow. (**a**) Mean contour map; (**b**) Contour map of inhomogeneity values.

namely slug flow and pseudo-slug flow. Their interface structure is shown in Fig. 13. Slug flow occurs at low superficial gas velocities and high liquid holdup, and the liquid slug completely occupies the cross-section of the pipeline. Pseudo-slug flow occurs at high superficial gas velocities. There is a strong interaction between the gas and the liquid at the elbow, so that a large number of bubbles are involved in the liquid slug. This makes the pseudo-slug flow look as if there is an apparent gas space above the liquid slug. It can be seen from Fig. 13 that whether the slug flow occurs at low superficial gas velocity or the pseudo-slug flow occurs at high superficial gas velocity, the flow process has obvious periodicity. In this paper, the cycle period of slug flow is divided into four stages, which are liquid accumulation, slug generation, slug eruption and liquid fallback. These four stages are specifically described as follows.

Liquid accumulation: The liquid moves along the upward-inclined pipe by the action of gas, and collides with the reflux liquid during the movement, resulting in an interface wave. The flow law of slug flow and pseudo-slug flow in this stage is similar.

Slug generation: The increase in the height of the liquid at the interface wave leads to a smaller cross-sectional region for the gas to pass through, an increase in the gas flow rate, and a smaller gas pressure, and the wave is easily adsorbed to the upper wall surface, at this time the cross-section of the pipeline is blocked by the liquid and a liquid slug is generated. Compared with the slug flow, the liquid slug of the pseudo-slug flow has a higher void fraction.

Slug eruption: In the slug flow, the gas is compressed due to the blockage of the cross-section. When the pressure increases to a certain value, the gas will enter the liquid slug. At this time, the liquid slug is sheared open to form a path through which the gas passes. When the gas flows out of the liquid slug, the pressure decreases and the compressed gas expands dramatically, driving the liquid to rise and deposit continuously, which is a violent high-speed eruption state.

Liquid fallback: At this time the slug eruption is completely over, and the liquid falls back and accumulates to form a new liquid

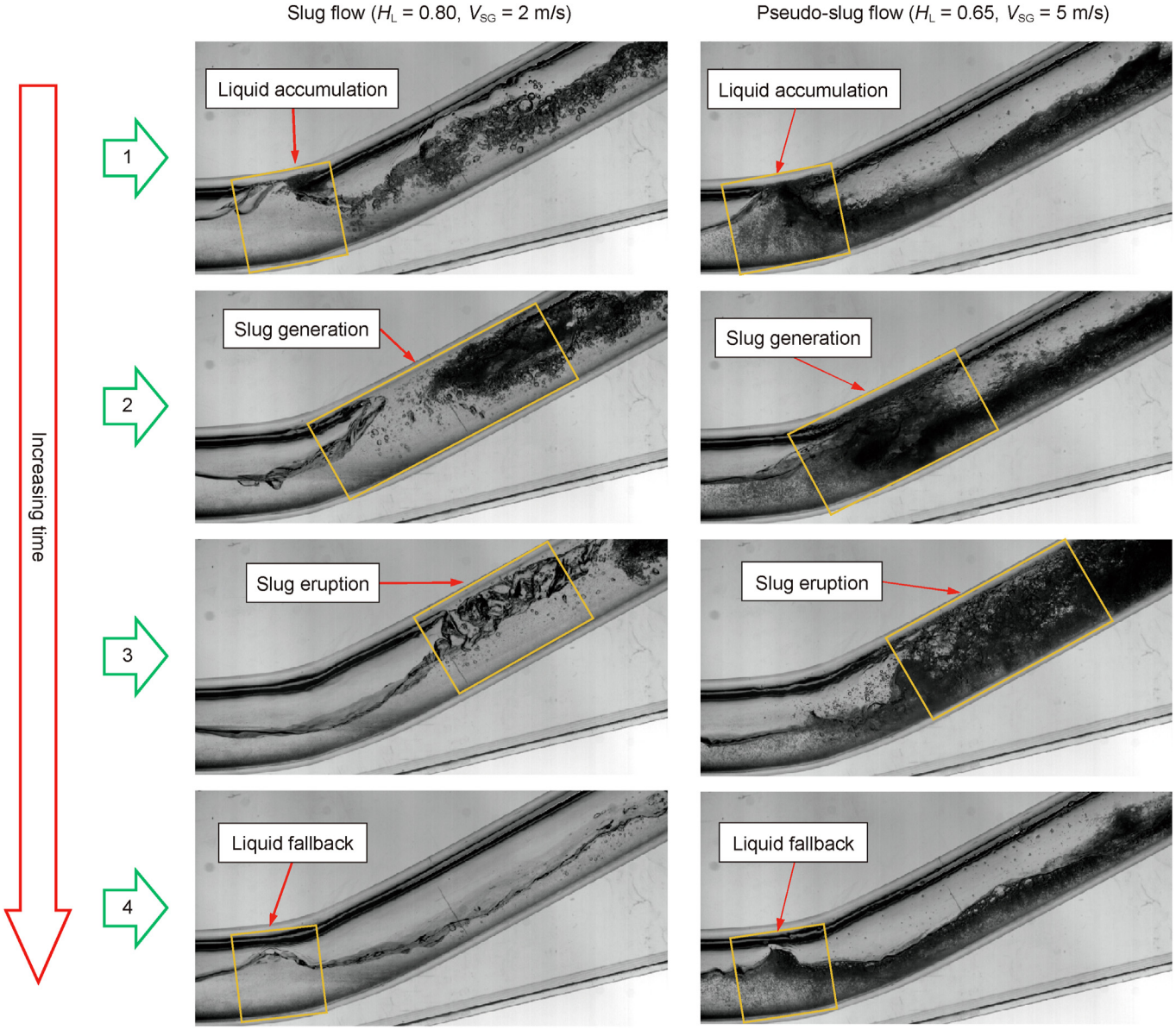

Fig. 13. Interface structure of two slug sub-flow patterns.

bridge, starting the next cycle period. The flow law of slug flow and pseudo-slug flow in this stage is similar.

The process of formation of slug flow at the elbow of zero net liquid flow can be represented by the geometry shown in Fig. 14(a). The initial accumulated liquid is a static water layer, which is a stratified flow at low superficial gas velocity, and the accumulated liquid flows along the bottom of the pipeline by the action of the gas. The vertical height of the liquid along the central line is h_L, and the perimeter of the interface is S_i. The perimeters of the pipes in contact with the gas and the liquid are S_G and S_L, respectively. The actual cross-sections of the pipe occupied by the gas and the liquid are A_G and A_L, respectively. Their specific calculations are as follows:

$$S_L = D\cos^{-1}\left(1-\frac{2h_L}{D}\right) \tag{18}$$

$$S_G = D\left[\pi-\cos^{-1}\left(1-\frac{2h_L}{D}\right)\right] \tag{19}$$

$$S_i = \sqrt{D^2-(D-2h_L)^2} \tag{20}$$

$$A_L = \frac{D^2}{4}\cos^{-1}\left(1-\frac{2h_L}{D}\right)-\frac{1}{2}\left(\frac{D}{2}-h_L\right)\sqrt{D^2-(D-2h_L)^2} \tag{21}$$

$$A_G = \frac{D^2}{4}\left[\pi-\cos^{-1}\left(1-\frac{2h_L}{D}\right)\right]+\frac{1}{2}\left(\frac{D}{2}-h_L\right)\sqrt{D^2-(D-2h_L)^2} \tag{22}$$

When the initial liquid holdup H_L is determined, h_L is also determined and their conversion relationship is:

$$H_L = \frac{\cos^{-1}\left(1-\frac{2h_L}{D}\right)-\left(1-2\frac{h_L}{D}\right)\sqrt{1-\left(1-2\frac{h_L}{D}\right)^2}}{\pi} \tag{23}$$

A study of Taitel et al. (1978) about solitary waves at the gas-liquid interface shows that when the liquid level h_L in the pipe is high, the interface wave driven by the gas reaches the top of the pipe and blocks the gas flow, and the stratified flow transitions to slug flow. Based on this conclusion, this paper considers the case of stratified flow of gas between flat plates as shown in Fig. 14(b). When the gas velocity increases, the gas pressure above the wave decreases due to the Bernoulli effect. This will cause the amplitude of the wave to increase, and the gravity acting on the wave will attenuate the wave. At this time, the infinite small amplitude wave stability criterion of the flow between plates is:

$$V_G > \left[\frac{g(\rho_L-\rho_G)h_G}{\rho_G}\right]^{\frac{1}{2}} \tag{24}$$

where h_G is the distance between the upper plate and the equilibrium liquid surface. This theory is further generalized to the finite wave case of stratified flow in a pipe. Consider a finite isolated wave on a flat-water surface as shown in Fig. 14(b). The peak height is h_L', the gas phase gap is h_G', and the gas phase gap and liquid phase gap of the equilibrium interface are h_G and h_L, respectively. The wave growth condition at this time is:

$$P-P' = (h_G-h_G')(\rho_L-\rho_G)g \tag{25}$$

From the Bernoulli equation:

$$P-P' = \frac{1}{2}\rho_G\left(V_G'^2-V_G^2\right) \tag{26}$$

The stability criterion at this time becomes:

$$V_G = C_1\left[\frac{g(\rho_L-\rho_G)h_G}{\rho_G}\right]^{\frac{1}{2}} \tag{27}$$

where C_1 depends on the size of the wave, the equation is:

$$C_1 = \left[\frac{2}{\frac{h_G}{h_G'}\left(\frac{h_G}{h_G'}+1\right)}\right]^{\frac{1}{2}} \tag{28}$$

For infinitesimal perturbations, $h_G/h_G' \to 1.0$ and $C_1 \to 1.0$, Eq. (27) can be simplified to Eq. (24). However, the comparison of these two equations shows that the finite perturbation is not as stable as the infinitesimal perturbation, because the value of the finite perturbation C_1 is less than 1. The theoretical analysis is further extended to the inclined circular pipe flow:

$$V_G = \left[\frac{2(\rho_L-\rho_G)g\cos\beta(h_L'-h_L)}{\rho_G}\cdot\frac{A_G'^2}{A_G^2-A_G'^2}\right]^{\frac{1}{2}} \tag{29}$$

For a finite small perturbation in a horizontal pipe, A_G' can be expanded into the Taylor series around A_G, and Eq. (29) can be rewritten as:

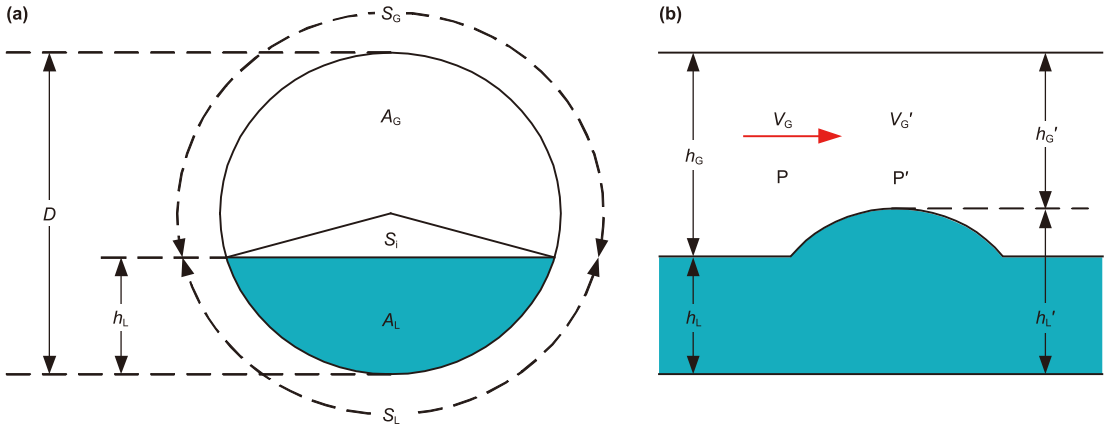

Fig. 14. Schematic diagram of the slug generation process at the gas-liquid interface. (**a**) Schematic diagram of pipe cross section; (**b**) Schematic diagram of pipe axial direction.

$$V_G = C_2\sqrt{\frac{(\rho_L-\rho_G)gA_G}{\rho_G\frac{dA_L}{dh_L}}} \tag{30}$$

where $C_2 \approx A_G'/A_G$. For the infinitesimal perturbation of $A_G' \to A_G$, the C_2 value is 1. When the equilibrium liquid surface is close to the top of the pipe and A_G is small, any finite amplitude fluctuation that occurs will cause $C_2 \approx A_G'/A_G$ to converge to 0. On the contrary, for the low equilibrium liquid surface, the presence of small finite amplitude waves has little effect on the size of the gas phase gap, and C_2 is close to 1.0. Thus C_2 is calculated as follows:

$$C_2 = 1-\frac{h_L}{D} \tag{31}$$

It can be obtained from calculus ideas:

$$\frac{dA_L}{dh_L} = S_i = \sqrt{D^2-(D-2h_L)^2} \tag{32}$$

For zero net liquid flow, the average gas phase velocity V_G and the superficial gas velocity V_{SG} satisfy:

$$V_G A_G = V_{SG} A \tag{33}$$

After substitution the criterion becomes:

$$\left(1+\frac{A_L}{A_G}\right)V_{SG} = \left(1-\frac{h_L}{D}\right)\sqrt{\frac{(\rho_L-\rho_G)gA_G}{\rho_G\frac{dA_L}{dh_L}}} \tag{34}$$

Since there is zero net liquid flow in this paper, the resulting interfacial waves tend to be smaller than in the case of simultaneous gas-liquid flow. Therefore, Eq. (34) can be rewritten to apply to the case of zero net liquid flow:

$$\left(1+\frac{A_L}{A_G}\right)V_{SG} = n\left(1-\frac{h_L}{D}\right)\sqrt{\frac{(\rho_L-\rho_G)gA_G}{\rho_G\frac{dA_L}{dh_L}}} \tag{35}$$

where n is the weakening factor and $n < 1.0$. Substituting Eqs. (21)–(23) and (31) and (32) into Eq. (35), the model is solved to be in good agreement with the experimental data when $n = 0.35$, as shown in Fig. 15. The model in this paper can accurately predict the boundary of the transition from stratified flow to slug flow at the elbow of zero net liquid flow.

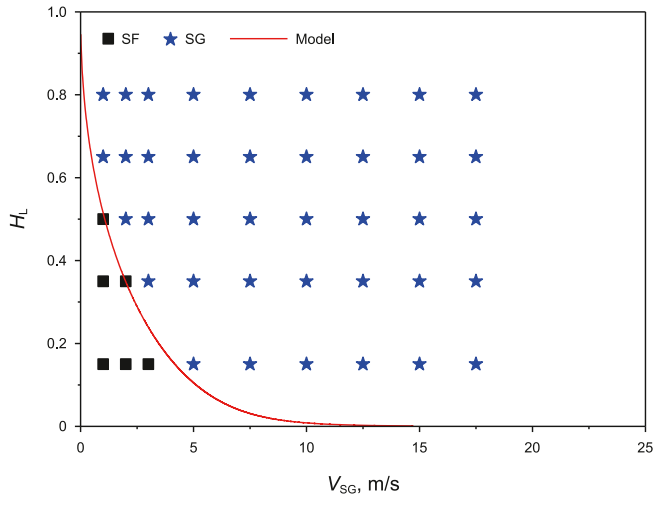

Fig. 15. Transition boundary between stratified flow and slug flow of zero net liquid flow.

There is also interphase mass transfer between gas and liquid in zero net liquid flow. When the superficial gas velocity is high, the gas will bring some liquid into the gas flow, and the gas will also penetrate into the liquid film to form bubbles. By the action of the gas phase, the liquid film and droplets are equipped with the ability to move, which is the essence of the accumulated liquid being taken out of the hilly terrain pipeline. During the transition from slug flow to stratified entrained flow, the gas entrainment droplets lead to the thinning of the liquid film until the accumulated liquid is completely carried out of the pipeline. Based on the visualization measurement results, the entrained droplets generated in the transition process of the slug flow to the stratified entrained flow in this paper are studied. The generation of entrained droplets is classified into four types, which are interfacial wave-type entrainment, bubble bursting-type entrainment, droplet impact-type entrainment, and liquid flooding-type entrainment.

The generation of splashing droplets by the impact of the airflow on the liquid is the most common way of producing entrained droplets observed in experiments. At different superficial gas velocities, the interfacial wave shows different kinematic properties. As shown in Fig. 16, the liquid film on the pipe wall observed in the experiment can be divided into two distinct regions: the wave and the basal liquid film. The wave is not on the same datum plane as the basal liquid film, and the wave forms peaks and valleys, or higher or lower than the basal liquid film.

In the experiment, it is found that the type of droplet entrainment caused by the interface wave motion at zero net liquid flow is shown in Fig. 17. Interface wave type entrainment is divided into three types: interface wave shear entrainment, interface wave root cutting entrainment and interface wave collision entrainment.

As shown in Fig. 17(a), when the interface wave shear entrainment occurs, the destruction of the wave by the airflow is shear. Accumulated liquid is affected by the gas to form several interfacial waves, at this time the gas velocity is much higher than the liquid film velocity. The wave peak is stretched and deformed along the flow direction by the action of the gas flow, and the gas forms an impact on the convex wave peak. Due to the existence of small bubbles, the stability of the wave is reduced, and it is easy to break into small droplets by gas (Zhang et al., 2019). As shown in Fig. 17(b), when the axial size of the wave is long enough, the airflow directly acts on the root of the interface wave, which causes the liquid volume at the peak to be much larger than that at the root. By the action of the airflow, the whole interface wave breaks from the root to form a large liquid block, which is further broken to form a small droplet. Since the shape of the wave is similar to the structure of the pocket, this entrainment droplet generation method is also called pocket breakup in the study of Zhang et al. (2019). As shown in Fig. 17(c), when adjacent waves collide, they recombine to form a similar banded structure. At this time, by the action of gas, the band will break and produce entrained droplets. This type of entrained droplet generation is also called band

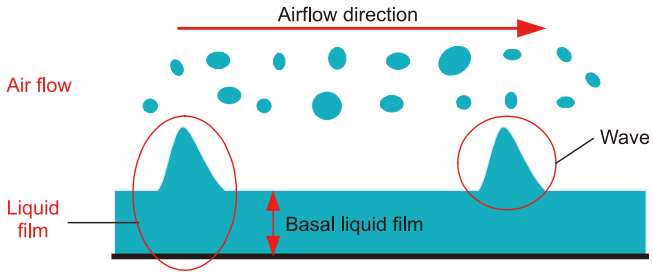

Fig. 16. Schematic diagram of wave and basal liquid film.

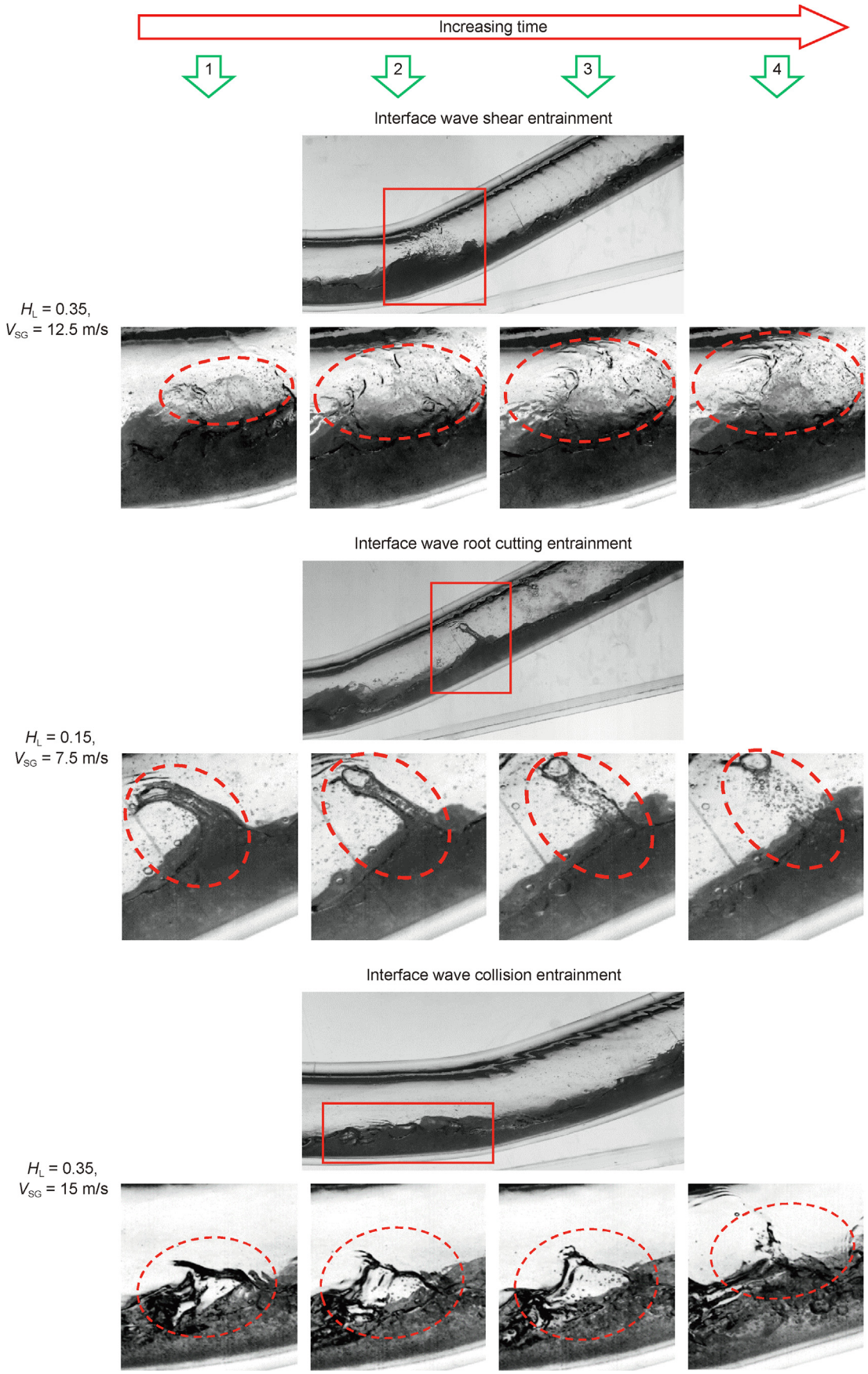

Fig. 17. Three types of interface wave entrainment.

breakup in the study of Zhang et al. (2019).

Part of the gas will enter the liquid film to produce bubbles, then gradually move from the inside of the liquid film to the gas-liquid interface, and finally break up to produce entrained droplets, this process is shown in Fig. 18. After the bubble reaches the gas-liquid interface, it first bulges at the interface to form a hemispherical cap. The liquid at the hemispherical cap becomes thinner by the action of the internal pressure of the bubble, and deforms by the action of the pressure difference, then ruptures to form small droplets. Hewitt (2013) also observed the phenomenon of droplet entrainment caused by bubble breakup in the liquid film.

As shown in Fig. 19, there is a liquid film formed by the aggregation of droplets on the upper wall of the upward-inclined pipe. Since the area of the liquid film is larger than the contact area of the droplets, the droplets with large momentum will form small droplets when they directly impact the liquid film, and provoke small droplets at the impact edge of the liquid film. Since the droplet collides with the surface of the liquid film, it is similar to the crater formed by the meteorite impacting the surface of the celestial body. This phenomenon is also called crater impact (Zhang et al., 2019).

As shown in Fig. 20, due to the insufficient liquid carrying capacity of the gas, the liquid begins to reflux, and the flow direction of the gas and the reflux liquid is opposite. When the interface wave amplitude of the liquid film on the upper and lower walls of the pipeline is large enough to meet the conditions of liquid flooding, a liquid bridge will be formed. The liquid bridge is torn into a large droplet block by the airflow, and the droplet block is further broken to form an entrained droplet.

In the process of slug flow transition to stratified entrained flow, the liquid is finally taken away from the upward-inclined pipe in the form of entrained droplets. The successful removal of accumulated liquid from hilly terrain pipelines depends on the ability of the high-velocity gas to carry away all of the entrained droplets. Therefore, the critical case is the equilibrium of forces on the droplets in the airflow, as shown in Fig. 21.

Taitel et al. (1980) pointed out that for the gas-liquid flow in an inclined pipe, when the gas velocity in the center of the pipe is large enough, the entrained droplets will produce an annular flow. At this time, the transition criterion from slug flow to annular flow is:

$$V_{SG} = m\left[\frac{\sigma(\rho_L-\rho_G)\sin\beta}{\rho_G}\right] \tag{36}$$

where σ is the surface tension of the liquid and $m = 3.1$ in the conventional two-phase flow. For zero net liquid flow, the departure of the accumulated liquid occurs in the upward-inclined pipe, and the slug flow transitions to a stratified entrained flow. Thus the transition boundary between the slug flow and the stratified entrained flow at zero net liquid flow can be obtained:

$$V_{SG} = 8.9\left[\frac{\sigma(\rho_L-\rho_G)\sin\beta}{\rho_G}\right] \tag{37}$$

As shown in Fig. 22, the modified model is in good agreement with the experimental data, and can accurately predict the right boundary of the slug flow in the zero net liquid flow.

3.4. Slug frequency

Slug frequency is a critical parameter of slug flow, which can influence the design and operation of pipeline system. For example, when designing a slug catcher and setting the working pressure, temperature and flow rate of the corresponding upstream pipeline, the slug frequency should be considered to meet its processing capacity.

Based on the image analysis method in Section 2.2, the frequency domain eigenvalues of the similarity signal curves for different superficial gas velocities can be analyzed. It can be seen from Fig. 23(a) that the frequency domain mean of the similarity signal increases first and then decreases at different initial liquid

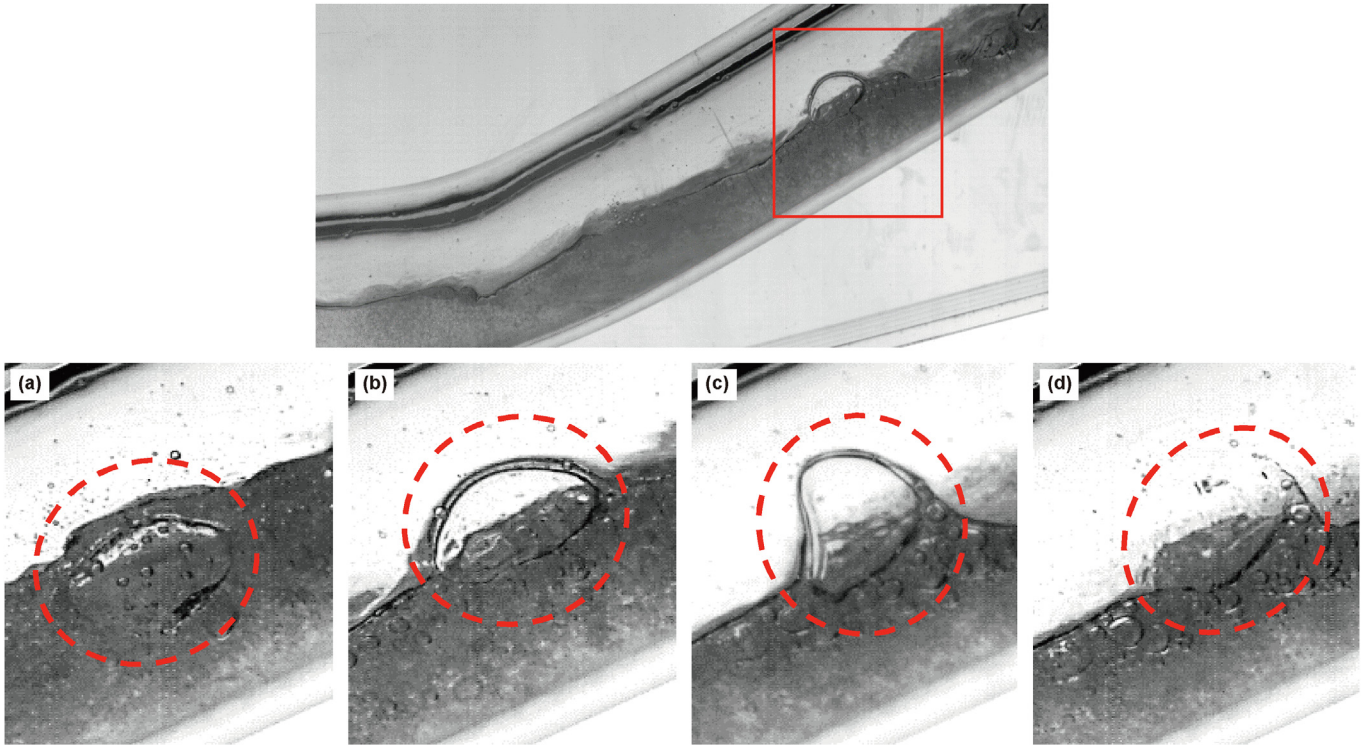

Fig. 18. Bubble breakup type entrainment ($H_L = 0.8$, $V_{SG} = 3.0$ m/s). (**a**) Beginning; (**b**) Process 1; (**c**) Process 2; (**d**) End.

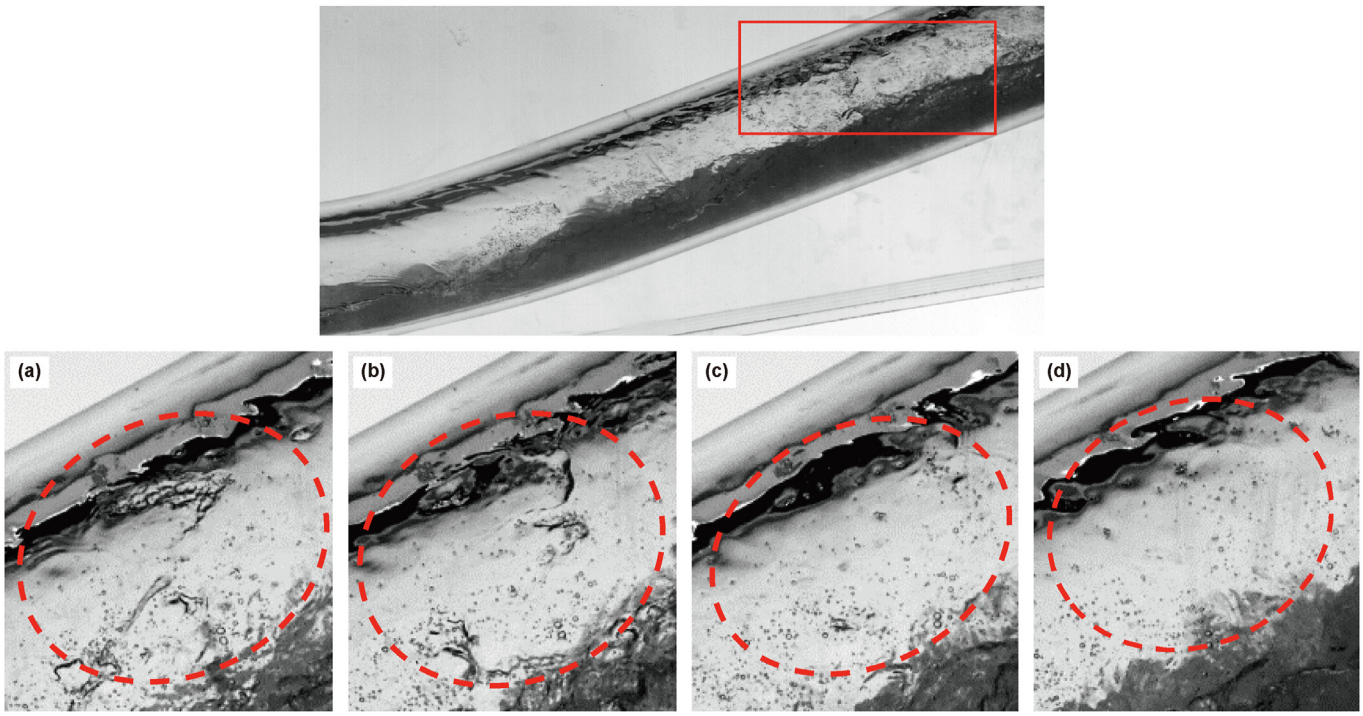

Fig. 19. Droplet impact type entrainment ($H_L = 0.15$, $V_{SG} = 15.0$ m/s). (**a**) Beginning; (**b**) Process 1; (**c**) Process 2; (**d**) End.

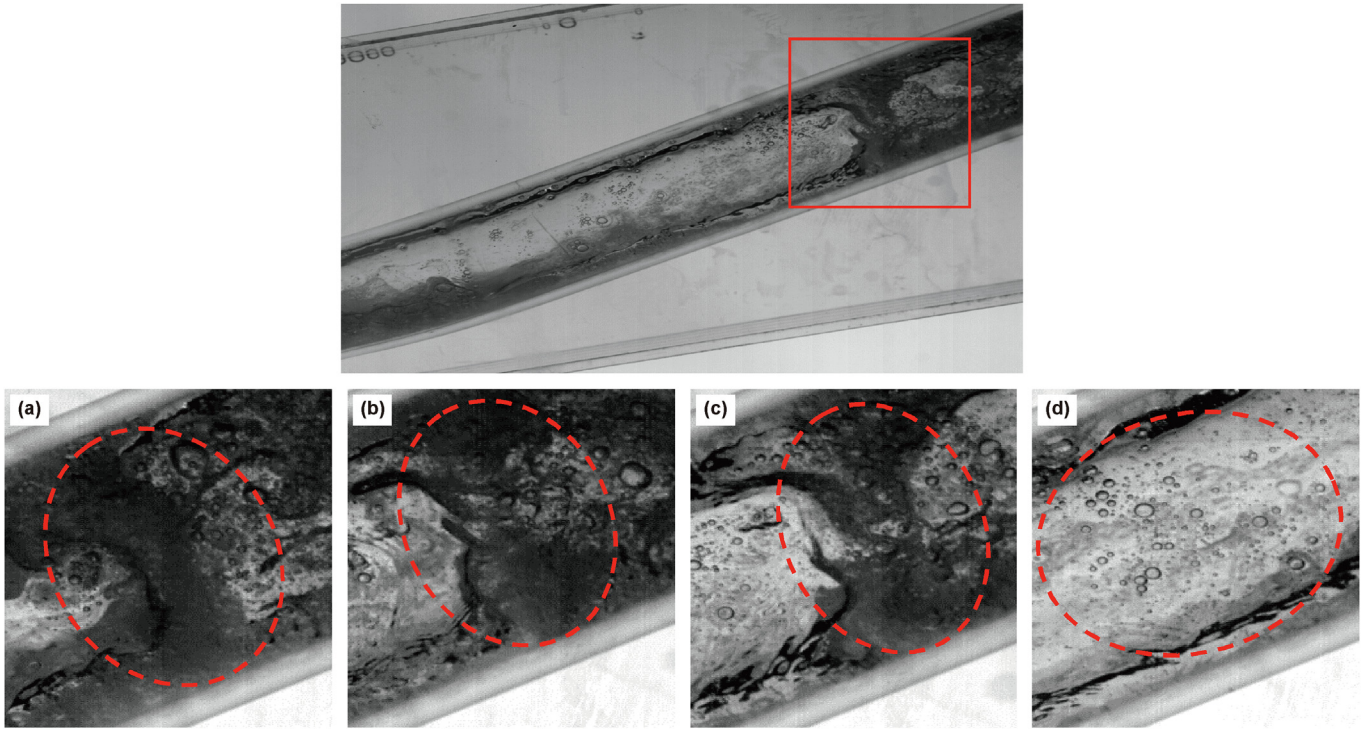

Fig. 20. Liquid flooding type entrainment ($H_L = 0.5$, $V_{SG} = 12.5$ m/s). (**a**) Beginning; (**b**) Process 1; (**c**) Process 2; (**d**) End.

holdups, and reaches a maximum at $V_{SG} = 7.5$ m/s. This is because the accumulated liquid continues to move from the horizontal pipe to the upward-inclined pipe as the superficial gas velocity increases. When $V_{SG} > 5.0$ m/s, the accumulated liquid in the horizontal pipe dries up, and the liquid holdup at the elbow is the highest. When $V_{SG} = 7.5$ m/s, the liquid has reflux, and the fluctuation of the interface is the largest and the mean value is the largest. And then the fluctuation of the interface starts to weaken as the accumulated liquid is continuously taken away from the pipe and the liquid holdup decreases. Therefore, when $V_{SG} > 7.5$ m/s, the mean value shows a decreasing trend.

The frequency range of 40 slug flow conditions in the experiment

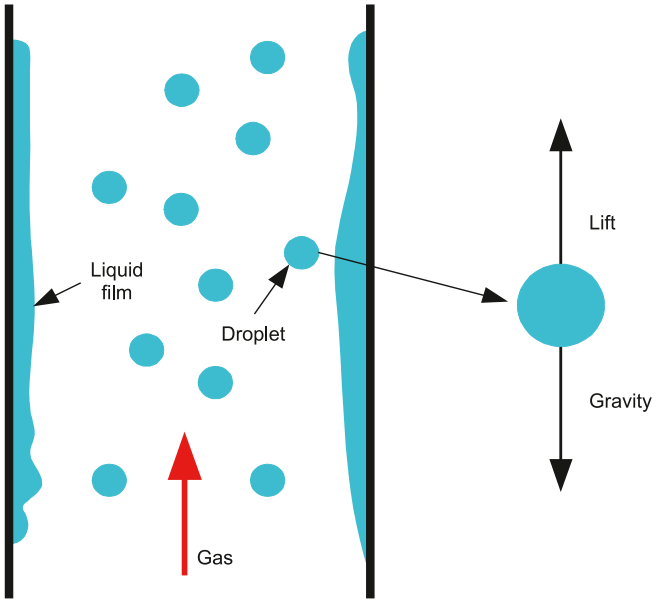

Fig. 21. Schematic diagram of force equilibrium for entrained droplets.

is 0.0–3.0 Hz. In this paper, the range of slug frequency is divided into six intervals on average, which are given in the histogram in the form of accumulation, and the variation of slug frequency with the superficial gas velocity is obtained, as shown in Fig. 23(b).

Researchers (Bernicot and Drouffe, 1991; Barnea and Taitel, 1993) found that the liquid slug length obeys the lognormal distribution in fully developed slug flow. Rodrigues et al. (2020) confirmed that the bubble translational velocity and slug frequency obey the Weibull distribution and logarithmic normal distribution, respectively. In this paper, the slug frequency distribution histogram of zero net liquid flow is fitted by a normal distribution, and the results are shown in Fig. 24. The equation is as follows:

$$\phi(f_s) = \frac{0.15}{0.38\sqrt{\frac{\pi}{2}}}\exp\left[-2\left(\frac{f_s-1.03}{0.38}\right)^2\right] + 0.05 \tag{38}$$

For Eq. (38), $R^2 > 0.9$ and the residual sum of squares $RSS < 0.01$. Therefore, the fitted correlation is in good agreement with the experimental data.

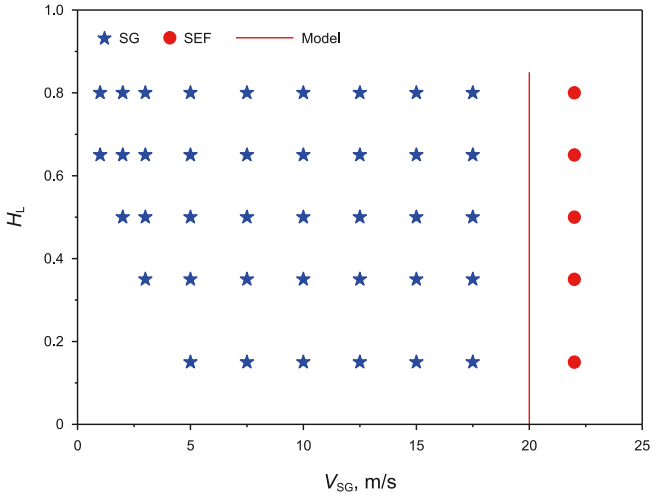

Fig. 22. Transition boundary between slug flow and stratified entrained flow in zero-net liquid flow.

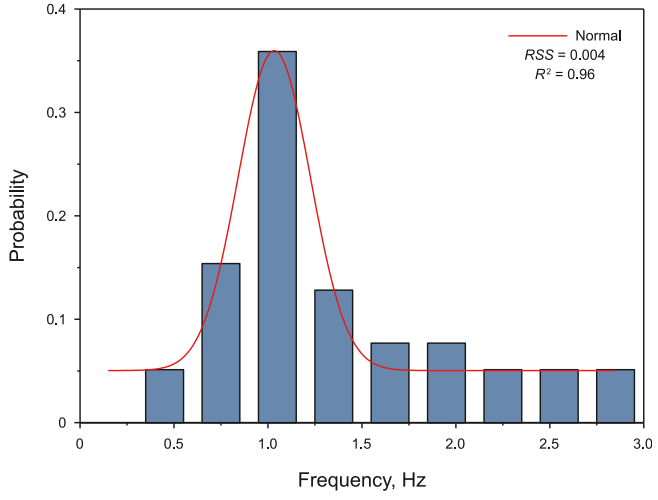

Fig. 24. Slug frequency normal distribution fitting of zero net liquid flow.

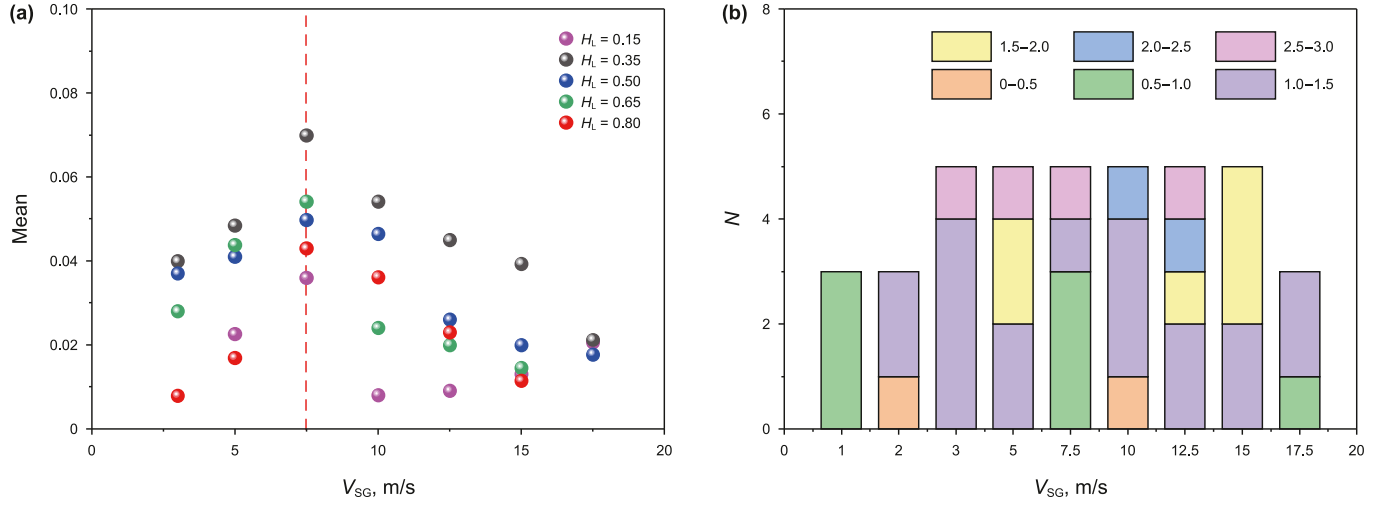

Fig. 23. The variation of slug flow frequency characteristics with superficial gas velocity. (**a**) The frequency domain mean varies with the superficial gas velocity; (**b**) Statistical distribution.

4. Conclusion

Liquid accumulation is easy to occur at the hilly terrain pipeline, which will have a great impact on the safety of oil and gas storage and transportation process. In this paper, the phenomenon of zero net liquid flow in a hilly terrain pipeline is studied, which is used to simulate the slug flow problem in the process of accumulated liquid removal. Based on the visual image at the elbow, the flow stages and flow patterns of the accumulated liquid were divided. The pressure drop distribution characteristics of the elbow are analyzed by the differential pressure signal, and it is found that the slug flow of the zero net liquid flow is essentially a periodic terrain induced slug. An image processing method is designed, which can process the complex transient interface information of zero net liquid flow and measure the slug frequency. However, for underwater signals, limited by the working environment, pressure signals are often used more widely. Finally, the flow pattern transition model is established, which can accurately predict the transition boundary of slug flow. The main conclusions of this paper are as follows.

(1) A method for dividing the flow stage of accumulated liquid related to the flow pattern is proposed. Based on the flow pattern generated by the elbow, the process of completely removing the accumulated liquid of zero net liquid flow is divided into four stages: liquid accumulation, liquid rising, continuous outflow, and tail outflow.
(2) The occurrence range of different flow patterns was quantitatively investigated. The pressure drop signal is analyzed from the time domain and frequency domain, and the dimensionless number-inhomogeneity value is introduced to draw the contour map of the pressure drop distribution. It is found that the inhomogeneity value of stratified flow is less than 0.12, the inhomogeneity value of stratified entrained flow is less than 0.07, and the inhomogeneity value of slug flow is between 0.12 and 0.54.
(3) It is found that the slug flow of zero net liquid flow is essentially a terrain-induced slug, and the slug flow is further divided into slug flow and pseudo-slug flow according to the mechanism of liquid slug generation. A boundary prediction model for the transition of stratified flow to slug flow is established, which can accurately predict the left boundary when slug flow occurs.
(4) The generation of entrained droplets of zero net liquid flow is divided into four types: interface wave type entrainment, bubble breakup type entrainment, droplet impact type entrainment and liquid flooding type entrainment. Based on the critical conditions, a boundary prediction model for the transition of slug flow to stratified entrained flow is established, which can accurately predict the right boundary when slug flow occurs.
(5) According to the periodicity of the slug flow of zero net liquid flow, the slug flow is divided into four stages: liquid accumulation, slug generation, slug eruption and liquid fallback. In this paper, an image processing method is proposed, and the slug frequency is successfully predicted based on this method. The normal distribution is used to fit the slug frequency, and the predicted correlation shows good agreement with the experimental data.

CRediT authorship contribution statement

Bo Huang: Writing – original draft, Validation, Methodology, Investigation, Formal analysis, Data curation, Conceptualization. **Qiang Xu:** Writing – original draft, Validation, Supervision, Methodology. **Ying-Jie Chang:** Writing – original draft, Investigation, Data curation. **Ye-Qi Cao:** Software, Formal analysis. **Hai-Yang Yu:** Software, Formal analysis. **Yu-Wen Li:** Software, Formal analysis. **Lie-Jin Guo:** Supervision, Resources, Conceptualization.

Conflict of interest statement

We declare that we have no conflict of interest including financial, personal or other relationships with other people or organizations that can inappropriately influence our work within three years of beginning the submitted work.

Acknowledgments

This work is supported by the Basic Science Center Program for Ordered Energy Conversion of the National Natural Science Foundation of China (No. 52488201), and the National Natural Science Foundation of China (No. 52422606).

References

Abdulkadir, M., Hernandez Perez, V., Lowndes, I.S., Azzopardi, B.J., Brantson, E.T., 2014. Detailed analysis of phase distributions in a vertical riser using wire mesh sensor (WMS). Exp. Therm. Fluid Sci. 59, 32–42. https://doi.org/10.1016/j.expthermflusci.2014.07.010.

Al Safran, E., Sarica, C., Zhang, H.Q., Brill, J., 2005. Investigation of slug flow characteristics in the valley of a hilly-terrain pipeline. Int. J. Multiphas. Flow 31 (3), 337–357. https://doi.org/10.1016/j.ijmultiphaseflow.2004.11.002.

Amaravadi, S., Minami, K., Shoham, O., 1994. The effect of pressure on two-phase zero-net liquid flow in inclined pipes. In: SPE Annual Technical Conference and Exhibition. SPE-28544-MS.

Amaravadi, S., Minami, K., Shoham, O., 1998. Two-phase zero-net liquid flow in upward inclined pipes: experiment and modeling. SPE J. 3 (3), 253–260. https://doi.org/10.2118/50974-PA.

Arabi, A., Salhi, Y., Zenati, Y., Si-Ahmed, E.K., Legrand, J., 2020. On Gas-Liquid Intermittent Flow in a Horizontal Pipe: Influence of Sub-regime on Slug Frequency. Pergamon. https://doi.org/10.1016/j.ces.2019.115251.

Barnea, D., Taitel, Y., 1993. A model for slug length distribution in gas-liquid slug flow. Int. J. Multiphas. Flow 19 (5), 829–838. https://doi.org/10.1016/0301-9322(93)90046-W.

Bernicot, M.F., Drouffe, J.M., 1991. A slug-length distribution law for multiphase transportation systems. SPE Prod. Eng. 6 (2), 166–170. https://doi.org/10.2118/17864-PA.

Birvalski, M., Koren, G.B., Henkes, R., 2014. Experiments and modelling of liquid accumulation in the low elbow of a gas/liquid pipeline. In: BHR North American Conference on Multiphase Production Technology. BHR-2014-A4.

Bissor, E.H., Ullmann, A., Brauner, N., 2020a. Liquid displacement from lower section of hilly-terrain natural gas pipelines. J. Nat. Gas Sci. Eng. 73, 103046. https://doi.org/10.1016/j.jngse.2019.103046.

Bissor, E.H., Yurishchev, A., Ullmann, A., Brauner, N., 2020b. Prediction of the critical gas flow rate for avoiding liquid accumulation in natural gas pipelines. Int. J. Multiphas. Flow 130, 103361. https://doi.org/10.1016/j.ijmultiphaseflow.2020.103361.

Deng, D., Tu, D.Y., Dong, Y., Geng, L., Gong, J., 2014. Calculation of hydrate formation probability in wet-gas pipelines. CIE J. 65 (6), 2270–2275. https://doi.org/10.3969/j.issn.0438-1157.2014.06.043.

Fan, D., Gong, J., Zhang, S.N., Shi, G.Y., Kang, Q., Xiao, Y.Q., Wu, C.C., 2021. A transient composition tracking method for natural gas pipe networks. Energy 215, 119131. https://doi.org/10.1016/j.energy.2020.119131.

Gregory, G.A., Aziz, K., Nicholson, M.K., 1981. Gas-Liquid Flow in Upwards Inclined Pipe with Zero Net Liquid Production. Psig Annual Meeting. PSIG-8101.

He, G.X., Tang, D.D., Yin, B.B., Sun, L.Y., Ding, D.Q., Liang, Y.T., Liao, K.X., 2018. Comparison and analysis of drainage measures for draining accumulated water condensed from wet CBM and transported in surface gathering pipeline network. J. Nat. Gas Sci. Eng. 56, 281–298. https://doi.org/10.1016/j.jngse.2018.06.017.

He, Z.Y., He, L.M., Liu, H.X., Wang, D., Li, X.W., Li, Q.P., 2021. Experimental and numerical study on gas-liquid flow in hilly-terrain pipeline-riser systems. Discrete Dynam Nat. Soc. 2021, 1–15. https://doi.org/10.1155/2021/5529916.

Hewitt, G., 2013. Annular Two-Phase Flow. Pergamon press. https://doi.org/10.1016/C2009-0-06773-7.

Hong, B.Y., Li, X.P., Song, S.F., Chen, S.L., Zhao, C.L., Gong, J., 2020. Optimal planning and modular infrastructure dynamic allocation for shale gas production. Appl. Energy 261, 114439. https://doi.org/10.1016/j.apenergy.2019.114439.

Hong, B.Y., Liu, S.N., Li, X.P., Fan, D., Ji, S.P., Chen, S.H., Li, C.C., Gong, J., 2022. A liquid loading prediction method of gas pipeline based on machine learning. Pet. Sci. 19 (6), 3004–3015. https://doi.org/10.1016/j.petsci.2022.05.002.

Horii, K., Zhao, Y.H., Tomita, Y., 1997. High performance spiral air-flow apparatus for

purging residual water in a pipeline. ASME Fluids Engineering Division Summer Meeting.
Kaji, R., Azzopardi, B.J., Lucas, D., 2009. Investigation of flow development of co-current gas–liquid vertical slug flow. Int. J. Multiphas. Flow 35 (4), 335–348. https://doi.org/10.1016/j.ijmultiphaseflow.2009.01.004.
Lei, Y., 2015. Investigation on Droplet Entrainment Mechanism of Low Liquid Loading Gas-Liquid Two-phase Flow in Wet Gas Pipelines. Master Thesis. Xi'an Shiyou University.
Liang, C.Y., Xiong, W., Carriveau, R., Ting, S.K., Wang, Z.W., 2022. Experimental and modeling investigation of critical slugging behavior in marine compressed gas energy storage systems. J. Energy Storage 49, 104038. https://doi.org/10.1016/j.est.2022.104038.
Liang, C.Y., Xiong, W., Wang, H., Carriveau, R., Ting, S.K., Li, P., Wang, Z.W., 2023a. Identification and maximum impact force modeling investigation for critical slugging in underwater compressed gas energy storage systems. J. Energy Storage. 67, 107550. https://doi.org/10.1016/j.est.2023.107550.
Liang, C.Y., Xiong, W., Wang, M.L., Ting, S.K., Carriveau, R., Wang, Z.W., 2023b. Experimental and modeling investigation for slugging pressure under zero net liquid flow in underwater compressed gas energy storage systems. Appl. Sci. 13 (2), 1216. https://doi.org/10.3390/app13021216.
Liu, W., Jiang, S., Li, H.Z., 2022. Experimental study of liquid-carrying by swirling flow in a U-shaped tube. Exp. Therm. Fluid Sci. 130, 110479. https://doi.org/10.1016/j.expthermflusci.2021.110479.
Liu, W., Shang, J.F., Wang, H.S., Zhao, D.H., Zou, Y., 2021. Study on the segmental pigging process for the wet gas gathering and transportation pipelines of the Puguang gas field. J. Pressure Vessel Technol. 143 (6), 061801. https://doi.org/10.1115/1.4051513.
Magnini, M., Ullmann, A., Brauner, N., Thome, J.R., 2018. Numerical study of water displacement from the elbow of an inclined oil pipeline. J. Petrol. Sci. Eng. 1000–1017. https://doi.org/10.1016/j.petrol.2018.03.067.
Minami, K., Shoham, O., 1996. Pigging dynamics in two-phase flow pipelines: experiment and modeling. Int. J. Multiphas. Flow 22 (S1), 145–146.
Mo, S., Ashrafian, A., Johansen, S.T., 2013. Two phase flow prediction of fluid displacement operations. In: 8th International Conference on Multiphase Flow, ICMF 2013.
Moffat, R.J., 1988. Describing the uncertainties in experimental results. Exp. Therm. Fluid Sci. 1 (1), 3–17.
Nnabuife, S.G., Kuang, B.Y., Whidborne, J.F., Rana, Z., 2021a. Development of gas–liquid flow regimes identification using a noninvasive ultrasonic sensor, belt-shape features, and convolutional neural network in an S-shaped riser. IEEE Trans. Cybern. 53 (1), 3–17. https://doi.org/10.1109/TCYB.2021.3084860.
Nnabuife, S.G., Kuang, B.Y., Whidborne, J.F., Rana, Z., 2021b. Non-intrusive classification of gas-liquid flow regimes in an S-shaped pipeline riser using a Doppler ultrasonic sensor and deep neural networks. Chem. Eng. J. 403, 126401. https://doi.org/10.1016/j.cej.2020.126401.
Rastogi, A., Fan, Y.L., 2020. Experimental and modeling study of onset of liquid accumulation. J. Nat. Gas Sci. Eng. 73, 103064. https://doi.org/10.1016/j.jngse.2019.103064.
Rodrigues, R.L.P., Cozin, C., Naidek, B.P., Neto, M.M., Silva, M.D., Morales, R.M., 2020. Statistical features of the flow evolution in horizontal liquid-gas slug flow. Exp. Therm. Fluid Sci. 119, 110203. https://doi.org/10.1016/j.expthermflusci.2020.110203.
Scott, S.L., Kouba, G.E., 1990. Advances in slug flow characterization for horizontal and slightly inclined pipelines. In: SPE Annual Technical Conference and Exhibition. SPE-20628-MS.
Shen, F., Yan, Z.Y., Zhao, Y.H., Horii, K., 2002. Theoretical analysis of using airflow to purge residual water in an inclined pipe. Appl. Math. Mech. 23, 694–702. https://doi.org/10.1007/BF02437654.
Sunday, N., Settar, A., Chetehouna, K., Gascoin, N., 2023. Numerical modeling and parametric sensitivity analysis of heat transfer and two-phase oil and water flow characteristics in horizontal and inclined flowlines using OpenFOAM. Pet. Sci. 20 (2), 1183–1199. https://doi.org/10.1016/j.petsci.2022.10.008.
Taitel, Y., Barnea, D., Dukler, A.E., 1980. Modelling flow pattern transitions for steady upward gas-liquid flow in vertical tubes. AIChE J. 26 (3), 345–354. https://doi.org/10.1002/aic.690260304.
Taitel, Y., Lee, N., Dukler, A.E., 1978. Transient gas-liquid flow in horizontal pipes: modeling the flow pattern transitions. AIChE J. 24 (5), 920–934. https://doi.org/10.1002/aic.690240518.
Taitel, Y., Simkhis, M., Tevelev, A., Barnea, D., 2016. Transient gas liquid flow in hilly terrain pipelines. Int. J. Multiphas. Flow 86, 21–27. https://doi.org/10.1016/j.ijmultiphaseflow.2016.07.001.
Taitel, Y., 1986. Stability of severe slugging. Int. J. Multiphas. Flow 12 (2), 203–217. https://doi.org/10.1016/0301-9322(86)90026-1.
Wu, X., Niu, S.H., Li, C.J., 2021. The study of the dynamic response of the natural gas pipeline aerial crossing during pigging process: a Review. J. Fluid Struct. 105, 103339. https://doi.org/10.1016/j.jfluidstructs.2021.103339.
Xu, G.L., Cai, L.X., Ullmann, A., Brauner, N., 2012. Trapped Water Flushed by Flowing Oil in Upward-Inclined Oil Pipelines, vol. 45127. International Pipeline Conference, pp. 637–647.
Xu, G.L., Zhang, G.Z., Liu, G., Ullmann, A., Brauner, N., 2011. Trapped water displacement from low sections of oil pipelines. Int. J. Multiphas. Flow 37 (1), 1–11. https://doi.org/10.1016/j.ijmultiphaseflow.2010.09.003.
Xu, Q., Wang, X.Y., Liang, L., Zhu, Y.S., Zhang, X.M., Liu, C.Y., Guo, L.J., 2021. Identification of flow regimes using platform signals in a long pipeline with an S-shaped riser. Chem. Eng. Sci. 244, 116819. https://doi.org/10.1016/j.ces.2021.116819.
Xu, Q., Zhou, H.Z., Zhu, Y.S., Cao, Y.Q., Huang, B., Li, W.S., Guo, L.J., 2020. Study of identification of global flow regime in a long pipeline transportation system. Powder Technol. 362, 507–516. https://doi.org/10.1016/j.powtec.2019.12.018.
Xu, Z., Hu, T., Pang, X.Q., Wang, E.Z., Liu, X.H., Wu, Z.Y., Chen, D., Li, C.R., Zhang, X.W., Wang, T., 2022. Research progress and challenges of natural gas hydrate resource evaluation in the South China Sea. Pet. Sci. 19 (1), 13–25. https://doi.org/10.1016/j.petsci.2021.12.007.
Yang, Y., Li, J.B., Wang, S.L., Wen, C., 2018. Gas-liquid two-phase flow behavior in terrain-inclined pipelines for gathering transport system of wet natural gas. Int. J. Pres. Ves. Pip. 162, 52–58. https://doi.org/10.1016/j.ijpvp.2018.03.005.
Yin, P.B., Cao, X.W., Li, Y.H., Yang, W., Bian, J., 2018. Experimental and numerical investigation on slug initiation and initial development behavior in hilly-terrain pipeline at a low superficial liquid velocity. Int. J. Multiphas. Flow 101, 85–96. https://doi.org/10.1016/j.ijmultiphaseflow.2018.01.004.
Yin, P.B., Cao, X.W., Wu, C., Qin, S.S., Zhang, P., Bian, J., 2020. The effect of surfactants on the initiation and development of air–water slug flow in hilly terrain pipeline. Exp. Therm. Fluid Sci. 117, 110139. https://doi.org/10.1016/j.expthermflusci.2020.110139.
Yu, H.Y., Xu, Q., Cao, Y.Q., Huang, Bo, Wang, H.X., Guo, L.J., 2023. Characterizations of gas-liquid interface distribution and slug evolution in a vertical pipe. Pet. Sci. 20 (5), 3157–3171. https://doi.org/10.1016/j.petsci.2023.03.009.
Zhang, H.X., Qin, M., Liao, K.X., Wang, K., He, G.X., 2021. Pipe-soil vibration characteristics of natural gas pipelines during the pigging process. J. Nat. Gas Sci. Eng. 95, 104148. https://doi.org/10.1016/j.jngse.2021.104148.
Zhang, P., Cao, X.W., Yin, P.B., Guo, D., Li, X., Gao, Y.Y., Bian, J., 2022. Effects of foam on slug generation mechanism in a hilly terrain pipeline. J. Petrol. Sci. Eng. 214, 110547. https://doi.org/10.1016/j.petrol.2022.110547.
Zhang, Z.N., Wang, Z.Y., Liu, H., Gao, Y.H., Li, H., Sun, B.J., 2019. Experimental study on bubble and droplet entrainment in vertical churn and annular flows and their relationship. Chem. Eng. Sci. 206, 387–400. https://doi.org/10.1016/j.ces.2019.05.005.
Zheng, G.H., Brill, J.P., Shoham, O., 1996. An experimental study of two-phase slug flow in hilly terrain pipelines. Int. J. Multiphas. Flow 22 (S1), 146, 146.